

# Simply split SIMPs

Nicolás Bernal,<sup>1,2</sup> Xiaoyong Chu<sup>3</sup> and Josef Pradler<sup>3</sup>

<sup>1</sup>*Centro de Investigaciones, Universidad Antonio Nariño  
Cra 3 Este # 47A-15, Bogotá, Colombia*

<sup>2</sup>*ICTP South American Institute of Fundamental Research  
Instituto de Física Teórica, Universidade Estadual Paulista  
R. Dr. Bento Teobaldo Ferraz 271, 01140-070 São Paulo, Brazil*

<sup>3</sup>*Institute of High Energy Physics,  
Austrian Academy of Sciences, Nikolsdorfer Gasse 18, 1050 Vienna, Austria*

E-mail: [nicolas.bernal@uan.edu.co](mailto:nicolas.bernal@uan.edu.co), [xiaoyong.chu@oeaw.ac.at](mailto:xiaoyong.chu@oeaw.ac.at),  
[josef.pradler@oeaw.ac.at](mailto:josef.pradler@oeaw.ac.at)

**Abstract.** Dark Matter which interacts strongly with itself, but only feebly with the Standard Model is a possibility that has been entertained to solve apparent small-scale structure problems that are pertinent to the non-interacting cold Dark Matter paradigm. In this paper, we study the simple case in which the self-scattering rate today is regulated by kinematics and/or the abundance ratio, through the mass-splitting of nearly degenerate pseudo-Dirac fermions  $\chi_1$  and  $\chi_2$  or real scalars  $\phi_1$  and  $\phi_2$ . We calculate the relic density of these states in a scenario where self-scattering proceeds through off-diagonal couplings with a vector particle  $V$  (Dark Photon) and where the abundance is set through number-depleting 4-to-2 reactions in the hidden sector, or, alternatively, via freeze-in. We study the implications of the considered models and their prospect of solving astrophysical small-scale structure problems. We also show how the introduction of the (meta-)stable heavier state may be probed in future dark matter searches.

---

## Contents

<b>1</b>	<b>Introduction</b>	<b>1</b>
<b>2</b>	<b>Simple Models with Off-diagonal Interactions</b>	<b>3</b>
<b>3</b>	<b>Dark Matter Relic Abundance</b>	<b>4</b>
3.1	Pseudo-Dirac Dark Matter	6
3.2	Real Scalar Dark Matter	8
3.3	Relative Abundance of the States 1 and 2 at the Decoupling	8
<b>4</b>	<b>Astrophysical Implications of Split SIMPs</b>	<b>10</b>
4.1	Decaying DM after Decoupling	10
4.2	Self-scattering of SIMPs	12
4.3	Free Streaming	13
<b>5</b>	<b>Sensitivity and Constraints on the Kinetic Mixing Portal</b>	<b>14</b>
<b>6</b>	<b>Conclusions and Outlook</b>	<b>16</b>
<b>A</b>	<b>Annihilation Rates</b>	<b>18</b>
<b>B</b>	<b>Solution to the Boltzmann Equation</b>	<b>19</b>
<b>C</b>	<b>Decay Rates and Self-scattering Cross Sections</b>	<b>19</b>
<b>D</b>	<b>Exothermic DM-Electron Scattering</b>	<b>20</b>

---

## 1 Introduction

The non-gravitational nature of Dark Matter (DM) remains a mystery. Yet, the apparent similarities in the cosmic abundances of DM and baryonic matter [1],  $\Omega_{\text{DM}} \simeq 5 \Omega_{\text{B}}$ , may be considered as indicative that both forms of matter were once in thermal equilibrium with each other. If so, this demands a minimum strength in coupling between the Standard Model (SM) and the hidden sector, restricting severely the class of models that hosts a successful DM candidate. In the past, this class of models has received by far the biggest attention, theoretically as well as experimentally. Most prominent in this class are extensions of SM that feature weakly interacting massive particles (WIMPs) as DM. WIMPs carry electroweak-scale mass and couple to SM with a strength that is reminiscent to that of the weak interactions. The correct relic density is then achieved in the chemical decoupling process from the SM.

Once the link between the SM and DM is gradually severed, both sectors may never reach thermal equilibrium with each other. The requirement  $\Omega_{\text{DM}} \simeq 5 \Omega_{\text{B}}$  then becomes prone to initial conditions and the details of the cosmic history, but the spectrum of possibilities amplifies. One possibility is that the DM abundance is set entirely in the hidden sector. This has been entertained recently in strongly self-interacting DM models that annihilate in number-depleting 3-to-2 [2–19] or 4-to-2 interactions [20]: the so-called Strongly Interacting Massive Particle (SIMP) mechanism, where “strong” must not necessarily allude to a confining

dark force. Although chemical equilibrium with the observable sector is never reached, DM may still carry the imprint of the SM thermal bath through elastic scatterings that keep DM in kinetic equilibrium with SM. In fact, the latter is often imposed as a requirement to prevent DM particles in the final state of the number-violating annihilation process to act as hot DM, significantly modifying structure formation [21]. Finally, it is possible that the dark and observable sector never reach kinetic equilibrium. It is the case adopted in this work. The “coldness” of DM can then be ensured by allowing the initial DM temperature  $T'$  to be much smaller than the SM temperature  $T$  [12, 20, 22].<sup>1</sup> Such initial condition can, *e.g.*, be dynamically achieved through a feeble coupling between DM and SM particles, through a hierarchy in branching-ratios in inflaton decay, or, more generally, by heating the SM sector through the decays of some exotic particles.

Although laboratory signatures of DM are less certain in the latter “non-WIMP”-type of models, elastic self-interactions of DM have consequences for structure formation. Models of SIMP DM have therefore been entertained as a solution to the small scale structure problems, which appear to persist in the collisionless DM paradigm, such as the “core vs. cusp problem” [23–26] and the “too-big-to-fail problem” [27, 28]. These can be alleviated if at the scale of dwarf galaxies there exists a large self-scattering cross section,  $\sigma$ , over DM particle mass,  $m$ , in the range  $0.1 \lesssim \sigma/m \lesssim 10 \text{ cm}^2/\text{g}$  [29–37]. The self-scattering of DM particles leads to heat transfer that decreases the density contrast in the centers of DM halos turning cusps into cores and changing the subhalo abundance matching due to a lower halo concentration. Self-interacting DM therefore directly addresses the two small-scale problems [29–34, 37], while astrophysical solutions also exist [38–41]. Although this effect alone cannot efficiently reduce the formation rate of luminous galaxies in DM subhalos, it may still alleviate the “missing satellites problem” [42, 43] with help of more DM physics (*e.g.* warm or decaying DM) or baryonic feedback.<sup>2</sup> Finally, the non-observation of an offset between the mass distribution of DM and hot baryonic gas in the Bullet Cluster constrains the DM self-interaction cross section to  $\sigma/m < 1.25 \text{ cm}^2/\text{g}$  at 68% CL [48–50], *i.e.*, approximately 1 barn for 1 GeV DM mass. Similarly, recent observations of cluster collisions lead to the constraint  $\sigma/m < 0.47 - 2 \text{ cm}^2/\text{g}$  at 95% CL [51, 52].

Here we consider the scenario that SIMPs come in the form of a finely split mass doublet, where the ground state (state 1) and the heavier state (state 2) share a common  $\mathbb{Z}_2$  symmetry, stabilizing state 1. Depending on the mass splitting between the two states, the heavier one can be long-lived on cosmological time-scales. The scenario hence resembles “inelastic DM” [53] where, at tree-level, each state only scatters with its counterpart, but not with itself. As a result, the effect of DM self-scattering depends on the abundances of both states. This provides a new way to regulate the DM self-interaction, alleviating strong astrophysical constraints in certain cases. In practice, it is achieved by modifying either the DM annihilation rate or the lifetime of heavier state. In the case of a long-lived heavier state, it leads to a two-component DM model. In order to achieve strong enough self-interaction, we are concerned with nearly degenerate states with sub-GeV DM mass, hence distinct from both exothermic double-disk [54] and boosted DM [55]. Moreover, the existence of the heavier state in our scenario leaves distinguishable imprints in the low-redshift Universe, as well as in DM search experiments.

It is the purpose of this work to investigate the viability of the above scenario for

---

<sup>1</sup>Alternatively, one may consider an enlarged dark sector that contains additional relativistic states at the moment of the freeze-out [7, 8], thereby preventing the heating of DM during freeze-out.

<sup>2</sup>While latest observations [44, 45] tend to prefer the latter option, the problem remains unsettled [46, 47].

both scalar and fermion DM. In this scenario the dark and observable sectors carry distinct temperatures. Such difference in temperatures can *e.g.* be generated in a small branching from inflaton decay into DM [56, 57]. The dark sector then reached chemical equilibrium within its own sector, while remaining decoupled from the SM sector. Alternatively, a difference in temperatures could also be dynamically generated, via a small portal between DM and SM particles through freeze-in [20, 58, 59]. For maintaining a nearly decoupled dark sector, we assume that the dark particles only feebly couple to SM particles, via a vector portal coupling. Throughout the study, the vector  $V$  mediating the DM self-interaction is assumed to be heavier, so that Sommerfeld enhancement plays no role [60–62]. Note that the  $\mathbb{Z}_2$  symmetry between two states prohibits 3-to-2 self-interactions, but instead allows for 4-to-2 annihilation (or, alternatively, freeze-in) to generate the observed DM density.

The paper is organized as follows. In Sec. 2 we introduce simple models for finely split states. In Sec. 3 we discuss the generation of the DM relic abundance via the 4-to-2 annihilations (or freeze-in) for two scenarios: pseudo-Dirac and real scalar DM. Sec. 4 is devoted to the astrophysical implications of split SIMPs; searches for possible connections between the dark and the visible sectors are discussed in Sec. 5. The conclusions are presented in Sec. 6. Some formulæ used in this work are provided in the Appendices.

## 2 Simple Models with Off-diagonal Interactions

A natural and simple possibility to ensure the dominance of inelastic interactions in self-scatterings is through the mediation of a massive vector particle  $V_\mu$  when the components of a Dirac fermion  $\Psi$  are split by small Majorana masses  $m_L$ ,  $m_R$ , or the real and imaginary parts of a complex scalar  $\Phi$  by a mass-squared parameter  $m_\phi^2$ ,

$$\mathcal{L}_\Psi = \bar{\Psi} (i\not{D} - M_D) \Psi - \frac{m_L}{2} (\bar{\Psi}^c P_L \Psi + h.c.) - \frac{m_R}{2} (\bar{\Psi}^c P_R \Psi + h.c.), \quad (2.1)$$

$$\mathcal{L}_\Phi = |D_\mu \Phi|^2 + M^2 |\Phi|^2 + (m_\phi^2 \Phi^2 + h.c.) - V_\Phi. \quad (2.2)$$

Here,  $D_\mu \equiv \partial_\mu + ig_V V_\mu$  is the covariant derivative with gauge coupling  $g_V$ ,  $\Psi^c = C\bar{\Psi}^T$  denotes the charge conjugate state,  $P_{R,L} \equiv \frac{1}{2}(1 \pm \gamma^5)$  are chirality projectors and  $H$  is the SM Higgs doublet. The scalar potential of  $\Phi$  is given by

$$V_\Phi = \lambda_\Phi |\Phi|^4 + \frac{\lambda'_\Phi}{2} (\Phi^4 + h.c.) + \lambda_m |\Phi|^2 |H|^2 + (\lambda'_m \Phi^2 + h.c.) |H|^2. \quad (2.3)$$

As we are interested in the possibility of split DM, the quartic self-couplings,  $\lambda_\Phi$  and  $\lambda'_\Phi$ , are assumed to be negligible unless otherwise stated.

We assume  $m_{L,R} \ll M_D$  and  $m_\phi \ll M$  for which  $\Psi$  decomposes into two mass-diagonal Majorana states  $\chi_{1,2} = \chi_{1,2}^c$  and  $\Phi$  into two real scalar fields  $\phi_{1,2}$ ,

$$\chi_1 \simeq \frac{i}{\sqrt{2}} (\Psi - \Psi^c), \quad \chi_2 \simeq \frac{1}{\sqrt{2}} (\Psi + \Psi^c), \quad \Phi = \frac{1}{\sqrt{2}} (\phi_1 + i\phi_2). \quad (2.4)$$

For the fermion states  $\chi_{1,2}$  the mixing angle that diagonalizes the mass matrix is maximal ( $\pi/4$ ) up to corrections  $\delta \equiv (m_L - m_R)/(2M_D) \ll 1$ . The masses are given by

$$\text{Pseudo-Dirac } \chi_{1,2}: \quad m_{1,2} \simeq M_D \mp \frac{m_L + m_R}{2} + O(\delta), \quad (2.5)$$

$$\text{Scalar } \phi_{1,2}: \quad m_{1,2}^2 = M^2 \mp m_\phi^2. \quad (2.6)$$

We note in passing that a complex  $m_\phi$  would not lead to a similar  $O(\delta)$  term in the scalar case, and we set all mass parameters to be real. In the following it will be convenient to parametrize the model in terms of  $m \equiv m_1$  and  $\Delta m \equiv m_2 - m_1 > 0$ . The interactions in the mass eigenbasis read

$$\mathcal{L}_{\text{int}, \chi} = i g_V \bar{\chi}_1 \gamma^\mu \chi_2 V_\mu + \frac{g_V}{2} \delta (\bar{\chi}_1 \gamma^\mu \gamma^5 \chi_1 - \bar{\chi}_2 \gamma^\mu \gamma^5 \chi_2) V_\mu, \quad (2.7)$$

$$\mathcal{L}_{\text{int}, \phi} = g_V (\phi_1 \partial^\mu \phi_2 - \phi_2 \partial_\mu \phi_1) V_\mu + \frac{1}{2} g_V^2 (\phi_1^2 + \phi_2^2) V^2 - V_\Phi(\phi_1, \phi_2). \quad (2.8)$$

Finally, the Lagrangian for the new gauge boson is given by

$$\mathcal{L}_V = -\frac{1}{4} V_{\mu\nu} V^{\mu\nu} + \frac{m_V^2}{2} V^2 - \kappa V_\mu J_{\text{SM}}^\mu, \quad (2.9)$$

where in the last term we consider an effective coupling to a SM current  $J_{\text{SM}}^\mu$ . A particular prominent choice is the gauge kinetic mixing [63] of the  $V$  and hypercharge ( $Y$ ) field strengths,  $-\kappa/(2 \cos \theta_W) F_{\mu\nu}^Y V^{\mu\nu}$ . In the low-energy effective theory, the coupling to the electromagnetic current is most important and hence  $J_{\text{SM}}^\mu = e \sum_f q_f \bar{f} \gamma^\mu f$  above, with  $e$  being the electromagnetic gauge coupling and  $q_f$  the charge of SM fermion  $f$ . The coupling of  $V$  to the SM neutral current is suppressed by  $m_V^2/m_Z^2$  and thus negligible for  $m_V \ll m_Z$ . We hence refer to  $V$  as “dark photon” throughout the paper. In all cases, we also impose the condition  $m_V > m_1 + m_2$  to ensure efficient decay of  $V$  within the dark sector.

Before moving to the next section, we comment on diagonal interactions that may appear. On the one hand, in the fermionic case the mass splitting is typically generated by a vacuum expectation value of a doubly dark-charged scalar  $S$  with the interaction term  $S(\bar{\Psi}^c \Psi)$ , that leads to a diagonal interaction term proportional to the mass splitting  $\Delta m$ , *i.e.*  $m_L + m_R$ . For  $\Delta m \ll m$ , its contribution to the DM elastic scattering is typically much smaller than the one produced by box diagrams with the exchange of two  $V$  bosons. A similar conclusion holds for interactions proportional to  $\delta$ , *i.e.*, for the parity-violating difference between  $m_L$  and  $m_R$ . On the other hand, for scalar DM, the quartic couplings  $\lambda_\Phi, \lambda_{\Phi'} > 0$  in the scalar potential  $V_\Phi$  yield diagonal interactions. Throughout this work, we require them to be weaker than the ones induced by exchanging two  $V$  bosons (see below). This holds true when

$$\lambda_\Phi + \lambda_{\Phi'} \leq \mathcal{O}(10^{-3}) g_V^4 \left( \frac{2.5 m}{m_V} \right)^4. \quad (2.10)$$

Likewise, we assume  $\delta = 0$ , so that diagonal interactions do not play a role in either DM self-scattering or DM 4-to-2 annihilation.

### 3 Dark Matter Relic Abundance

We first study the generation mechanisms of the observed DM density, and how the relative abundance of states 1 and 2 is determined. Within the framework of standard cosmology, the final abundance of DM particles can be generated either via 4-to-2 annihilations or via freeze-in. We start with the former and discuss the latter towards the end of this section.

We assume that the dark sector (states 1, 2 and  $V$ ) was once in equilibrium with each other, so that we can define the relative abundance of states 1 and 2 by their corresponding ratio

$$R(T') \equiv \frac{n_2(T')}{n_1(T')} = \left( 1 + \frac{\Delta m}{m} \right)^{3/2} e^{-\frac{\Delta m}{T'}} \simeq e^{-\frac{\Delta m}{T'}}. \quad (3.1)$$

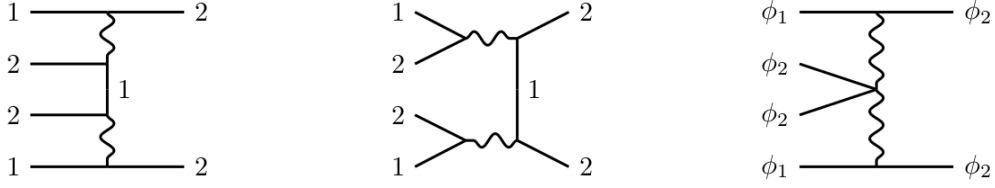


**Figure 1.** Exemplary 4-to-2 annihilation diagrams. The first two diagrams (left and central panels) are the only non-vanishing processes in the leading non-relativistic limit for pseudo-Dirac DM. For scalar DM there is a another topology (right panel) which involves a quartic gauge coupling that is diagonal in  $\phi_i$ .

Here  $T'$  denotes the dark sector temperature which is, in general, different from the photon temperature  $T$ . Eq. (3.1) is valid when both states are non-relativistic and share a common chemical potential, *i.e.*, while the  $11 \leftrightarrow 22$  reaction is in equilibrium. When considering finely split states  $\chi_{1,2}$  or  $\phi_{1,2}$  it is natural to solve for the sum of the respective number densities  $n \equiv n_1 + n_2 = n_1 (1 + R)$  in the relic density calculation. Let us point out that the  $11 \leftrightarrow 22$  reaction does not affect the total DM number density; nevertheless, the latter process is crucial to determine the value of  $R$  at late times.

In the SIMP mechanism, the final DM abundance is fixed by number-depleting processes, some of which are shown in Fig. 1. Quantitatively, the evolution of the dark-sector comoving number density is governed by the Boltzmann equation

$$\frac{dY}{dx} = -\frac{s^3 \langle \sigma v^3 \rangle_{4 \rightarrow 2}}{xH} (Y^4 - Y^2 Y_{\text{eq}}^2), \quad (3.2)$$

where  $x \equiv m/T$  and  $Y \equiv n/s$  is the yield variable, including both states 1 and 2, defined in terms of the SM entropy density  $s(T)$ .  $Y_{\text{eq}}$  denotes the equilibrium yield in the dark sector. The thermally averaged cross section is given by

$$\begin{aligned} \langle \sigma v^3 \rangle_{4 \rightarrow 2} \equiv \frac{1}{(1+R)^4} & \left[ \langle 2222 \rightarrow 11 \rangle R^4 + \langle 1222 \rightarrow 12 \rangle R^3 + (\langle 1122 \rightarrow 22 \rangle + \langle 1122 \rightarrow 11 \rangle) R^2 \right. \\ & \left. + \langle 1112 \rightarrow 12 \rangle R + \langle 1111 \rightarrow 22 \rangle \right]. \end{aligned} \quad (3.3)$$

The definition of the expressions  $\langle ijkl \rightarrow ab \rangle$  is detailed in Appendix A. Since  $Y$  describes the total abundance of both states 1 and 2, only total number-changing processes are taken into account, including co-annihilation channels. In this expression, the entropy density  $s$  and the Hubble rate  $H$  are functions of the temperature  $T$ , whereas  $R$  is a function of  $T'$  (or equivalently  $x' \equiv m/T'$ ). In our study, we solve the Boltzmann equation (3.2) numerically and obtain the freeze-out time and the DM relic abundance (see Appendix B).

As already pointed out in Ref. [3], if dark and visible sectors are decoupled, one can equivalently track the evolution from the separate conservation of respective comoving entropies  $S'$  and  $S$ . The DM abundance at freeze-out can then be estimated as [20]

$$\Omega_{\text{DM}} h^2 \sim \frac{m}{3.6 \text{ eV} (x'_{\text{FO}} + 2.5)} \frac{S'}{S}, \quad (3.4)$$

which in turn allows to determine the entropy ratio, from the observed DM relic abundance and for a given freeze-out point,  $x'_{\text{FO}}$ . In practice, the value of  $x'_{\text{FO}}$  is of order  $\mathcal{O}(15)$  (see left

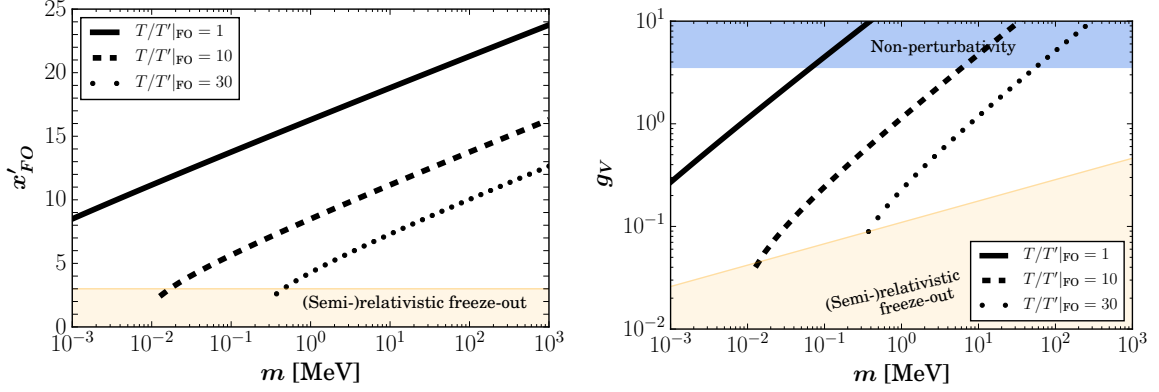


**Figure 2.** Pseudo-Dirac DM freeze-out in the non-relativistic regime as a function of the DM mass  $m$ , for  $\Delta m/m = 10^{-2}$  and various temperature ratios at DM freeze-out. The *left* panel shows the freeze-out point  $x'_{\text{FO}}$  that yields the observed DM density, while the *right* panel shows the corresponding value of the dark gauge coupling  $g_V$ , assuming  $m_V = 2.5 m$ .

panel of Fig. 2), so for each DM mass the final relic abundance is largely fixed by the entropy ratio, and vice versa.

Importantly, the fact that  $x'_{\text{FO}}$  cannot be arbitrarily large yields an upper bound on the entropy ratio, and thus on total extra energy density contributed by the dark sector. The latter is often quantified in the effective number of relativistic neutrino degrees of freedom,  $N_{\text{eff}}^\nu = 3.046 + \Delta N_{\text{eff}}^\nu$  where  $\Delta N_{\text{eff}}^\nu$  measures beyond SM contributions. Quantitatively, Eq. (3.4) together with separate entropy conservation suggest that

$$\Delta N_{\text{eff}}^\nu|_{\text{BBN}} \lesssim 10^{-2} \left[ \frac{x'_{\text{FO}} + 2.5 \text{ keV}}{16} \frac{1}{m} \right]^{\frac{4}{3}} \quad (3.5)$$

at  $T \sim 1 \text{ MeV}$ , assuming a relativistic dark sector at that moment. From Eq. (3.5) it follows that for DM heavier than a few keV, the dark sector does not contribute to extra radiation in quantities where it is currently constrained: the concordance of Big Bang Nucleosynthesis (BBN) predictions and observationally inferred primordial light element abundances of D and  $^4\text{He}$  imply  $N_{\text{eff}}^\nu = 2.88 \pm 0.16$  [64] (marginalized over the CMB determined baryon density). The scenario is also consistent with the CMB determination without BBN,  $N_{\text{eff}}^\nu = 3.15 \pm 0.23$  [1], because dark particles will have become non-relativistic at matter-radiation equality for  $m \gtrsim 1 \text{ keV}$ .

### 3.1 Pseudo-Dirac Dark Matter

For fermionic DM, the only non-vanishing S-wave annihilation process is  $2\chi_i + 2\chi_j \rightarrow 2\chi_i$  with  $i \neq j$ , due to the Pauli exclusion principle.<sup>3</sup> That is, the 4-to-2 interaction rate, Eq. (3.3), becomes

$$\langle \sigma v^3 \rangle_{4 \rightarrow 2} = [\langle 1122 \rightarrow 22 \rangle + \langle 1122 \rightarrow 11 \rangle] \frac{R^2}{(1+R)^4}, \quad (3.6)$$

<sup>3</sup>Here the term “S-wave” refers to vanishing angular momentum between any pair of the incoming particles.



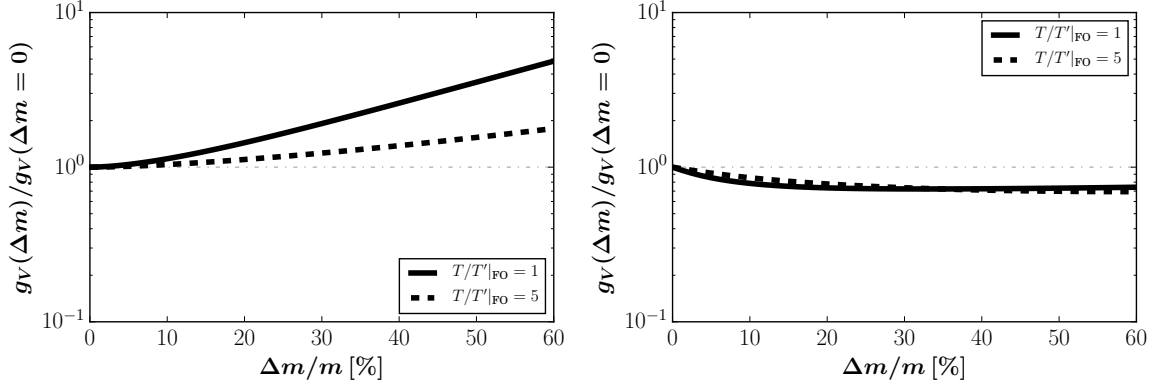


**Figure 3.** Gauge coupling  $g_V$ , derived from the observed relic DM abundance, as a function of the mass difference  $\Delta m/m$  for several fixed values of temperature ratios at freeze-out,  $T'/T|_{FO}$ . The left (right) panel is for fermion (scalar) DM with  $m = 10$  keV and  $m_V = \frac{5}{2}m + \Delta m$ ; only terms constant in relative velocities are considered.

being suppressed in the non-relativistic regime by the number density of state 2. In the previous equation, the two relevant annihilation cross sections are given by

$$\langle 1122 \rightarrow 11 \rangle = \langle 1122 \rightarrow 22 \rangle = \frac{27\sqrt{3}g_V^8 (m_V^4 - 8m^2m_V^2 - 8m^4)^2}{32\pi (m_V^4 - 2m^2m_V^2 - 8m^4)^4}, \quad (3.7)$$

up to corrections proportional to  $\Delta m$ . Typical diagrams contributing to the process are shown in the left and middle panels of Fig. 1. In the middle panel, if  $m_V = m_1 + m_2$  both vector propagators can simultaneously go on-shell, substantially enhancing the efficiency of the process. In our analysis, this resonance is never reached since  $m_V > m_1 + m_2$  has been imposed in order to have a rapid decay of  $V$  into states 1 and 2.

Figure 2 presents different aspects of the solution of the Boltzmann equation (3.2) in the non-relativistic regime: for several temperature ratios  $T/T'$  at freeze-out, the figure shows the freeze-out point (left panel) and the dark gauge coupling  $g_V$  (right panel) for achieving the measure DM abundance, as a function of the DM mass. The upper blue region, corresponding to  $g_V > \sqrt{4\pi}$ , goes beyond our perturbative approach. It is shown that for an increasing DM mass, a larger  $x'_{FO}$  (and hence a stronger Boltzmann suppression) is required in order to achieve the correct relic density. This implies a later freeze-out and in turn a stronger gauge interaction. A suppression of the DM yield can also be achieved by imposing a colder dark sector, where smaller values of  $x'_{FO}$  and  $g_V$  can produce the observed DM density. The right panel suggests the ballpark of interest for DM masses: for  $m \gtrsim$  GeV one faces the perturbativity limit; in turn, fermionic DM is also bounded from below,  $m \gtrsim 1$  keV, by the Gunn-Tremaine limit [65, 66]. For the remainder of this work we restrict ourselves to the keV-GeV mass bracket. In the lower regions of both panels, freeze-out proceeds when DM is (semi-)relativistic ( $x'_{FO} < 3$ ). There, the final DM abundance can be directly obtained from the temperature ratio, and independently of the gauge coupling  $g_V$  [67].

The left panel of Fig. 2 also shows that  $x'_{FO}$  is much smaller than the assumed value  $(\Delta m/m)^{-1} = 100$  for the entire parameter region. That is, the number density of state 2 remains relatively unsuppressed at freeze-out, which guarantees that S-wave annihilation dominates. This can also be seen from the left panel of Fig. 3, where we plot the values of  $g_V$  needed in order to produce the observed DM relic abundance through S-wave annihilation for



fermionic DM. For the plot, we choose  $m = 10$  keV and  $m_V = \frac{5}{2}m + \Delta m$ . It illustrates how the increase of  $\Delta m/m$  leads to a smaller S-wave annihilation rate, which in turn needs to be compensated by a larger  $g_V$ . Such a feature is more noticeable if the freeze-out happens later, *i.e.*, larger  $x'_{\text{FO}}$ , corresponding to higher masses or smaller  $T/T'|_{\text{FO}}$  (see left panel of Fig. 2). This can be understood from Eq. (3.1): larger  $x'_{\text{FO}}$  leads to stronger Boltzmann suppression in  $R$ . In practice, velocity suppressed contributions to annihilation do not become important until  $\Delta m/m \geq 10\%$  (20%) for  $T/T'|_{\text{FO}} = 1$  (5). Hence, for our purposes, it is safe to neglect them, as we will be mostly concerned with mass splittings  $\Delta m/m \lesssim 1\%$  in the following sections, which are phenomenologically more interesting.

### 3.2 Real Scalar Dark Matter

In a similar fashion as for pseudo-Dirac DM we obtain the solution to the Boltzmann equation for the two finely split real scalars  $\phi_{1,2}$ . The major difference is the absence of Pauli blocking in the initial state of four scalars; channels involving more than two identical particles in the initial state, such as  $3\phi_i + \phi_j \rightarrow \phi_i + \phi_j$  and  $4\phi_i \rightarrow 2\phi_j$ , with  $i \neq j$ , are now allowed. The cross sections read

$$\langle ijkl \rightarrow mn \rangle \simeq a_{ijkl} \frac{9\sqrt{3}}{32\pi} \frac{g_V^8}{(2m^2 + m_V^2)^4}, \quad (3.8)$$

where  $a_{1122} = 1$ ,  $a_{1111} = a_{2222} = 12$  and  $a_{1112} = a_{1222} = 4$ . As a result, the freeze-out process is not suppressed by either the number density ratio  $R$  or the relative velocity, *i.e.*, all the terms in Eq. (3.3) are present in this case.

The dependence of  $g_V$  on  $\Delta m/m$  for scalar DM freeze-out, using the same DM and vector masses as before, is illustrated in the right panel of Fig. 3. As can be seen, the required values of  $g_V$  to obtain the DM abundance is less sensitive to the mass difference for scalar DM. Once  $\Delta m/m \gtrsim 20\%$  annihilation via  $1111 \rightarrow 22$  becomes dominant while others become suppressed by  $R$ . Since the interaction rate of  $1111 \rightarrow 22$  is approximately independent of the value of  $\Delta m/m$  at freeze-out, so is  $g_V$ .

### 3.3 Relative Abundance of the States 1 and 2 at the Decoupling

In this subsection we discuss the abundance ratio  $R$  defined in Eq. (3.1), and especially its value  $R_{\text{dec}} \equiv R(T'_{\text{dec}})$  after the decoupling of the reaction  $22 \leftrightarrow 11$  at a dark sector temperature  $T'_{\text{dec}}$ . Its value today,  $R_0$ , will be discussed in Sec. 4.1; astrophysical implications in the low-redshift Universe depend critically on the latter. It is clear that  $R_0 = 0$  if the decay rate of state 2 satisfies  $\Gamma_2 \gg H_0$ , where  $H_0$  is the Hubble constant. However, if state 2 is meta-stable on cosmological timescales,  $\Gamma_2 \ll H_0$ , then  $R_0 \simeq R_{\text{dec}}$ .

In the SIMP mechanism studied above, where dark sector thermalizes in the early Universe,  $T'_{\text{dec}}$  is found from

$$n_2(T'_{\text{dec}}) \langle \sigma_{22 \rightarrow 11} v \rangle = n(T'_{\text{dec}}) \left[ \frac{R(T'_{\text{dec}})}{1 + R(T'_{\text{dec}})} \langle \sigma_{22 \rightarrow 11} v \rangle \right] = H(T_{\text{dec}}), \quad (3.9)$$

where  $n(T'_{\text{dec}})$  is fixed by the observed DM relic abundance. Note that the relation between  $T'_{\text{dec}}$  and  $T_{\text{dec}}$ , or equivalently, between the entropies of the two sectors, is given by the solution of the Boltzmann equation (3.2), as mentioned above. Due to its large cross section, the kinetic decoupling typically happens after the 4-to-2 freeze-out. Although it is difficult to solve the above equation analytically,  $R(T'_{\text{dec}})$  may be estimated as follows: given that  $n(T'_{\text{dec}})$  is fixed

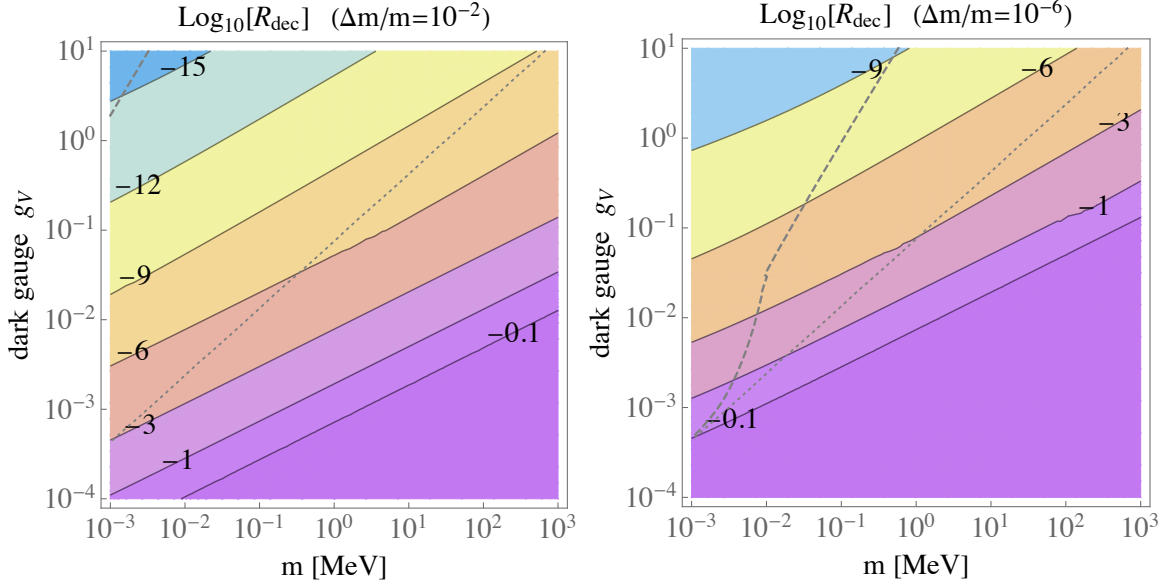


**Figure 4.** Contour lines for  $\text{Log}_{10}R_{\text{dec}}$  for fermionic DM with  $\Delta m/m = 10^{-2}$  (left panel) and  $10^{-6}$  (right panel), and  $m_V = \frac{5}{2}m$ . In the region below the contour  $-0.1$ ,  $n_1 \simeq n_2$  approximately holds. In each panel, dashed and dotted lines show  $R_0 \sigma_{12}/m = 1 \text{ cm}^2/\text{g}$  and  $\sigma_{12}/m = 1 \text{ cm}^2/\text{g}$ , respectively, assuming  $R_0 = R_{\text{dec}}$  (explained below). All the points reproduce the observed DM relic abundance.

by the observed DM abundance, the factor inside the square bracket in Eq. (3.9) should be close to the thermal annihilation cross section of ordinary WIMP DM at decoupling. That is,  $R_{\text{dec}} \sim \mathcal{O}(1) \text{ pb}/\langle\sigma_{22\rightarrow 11}v\rangle$ . Nevertheless, we caution the reader that this analogy fails once  $m/T'_{\text{dec}} \gg 25$ , or, in practice, when  $\Delta m/m \lesssim 10^{-2}$ , and in the following we solve Eq. (3.9) numerically.

Figure 4 shows the values of  $R_{\text{dec}}$  that result from fixing the freeze-out abundance to the observed DM relic density (by adjusting  $T/T'_{\text{FO}}$ ) for two different mass splittings:  $\Delta m/m = 10^{-2}$  (left panel) and  $10^{-6}$  (right panel). A large mass splitting results in a negligible abundance of state 2. On similar grounds, large values of  $R_{\text{dec}}$  are observed in the region of small  $g_V$  and large  $m$ . The latter combination corresponds to regions of small annihilation cross section, for which an appreciable number of particles of type 2 must be present to facilitate the 4-to-2 processes.  $R_{\text{dec}} \lesssim 1$  is only achieved when  $T'_{\text{dec}} \geq \Delta m$  and together with Eq. (3.9) this implies

$$g_V \lesssim 3 \times 10^{-4} \frac{m_V}{\sqrt{m \text{ MeV}}} \left( \frac{m^2}{\Delta m^2} \frac{m T'_{\text{FO}}}{T_{\text{FO}}^2} \right)^{\frac{1}{8}}, \quad (3.10)$$

where, again, the observed DM abundance has been used as an input.

Before ending this section, we comment on the case of the freeze-in via the production of  $V$  from SM.<sup>4</sup> If the DM abundance is generated by freeze-in, the DM number density is proportional to the portal interaction, as the latter transfers energy from the SM thermal bath to the dark sector.<sup>5</sup> Under the assumption that the dark sector is never thermalized,

<sup>4</sup>Freeze-in of on-shell dark photons has, *e.g.*, been calculated in detail in Ref. [68].

<sup>5</sup>Re-annihilation, as a mixture of freeze-in and number-depleting SIMP annihilation, is also possible [12]. Nevertheless, it only works for a very narrow parameter region, which will not be investigated here.

the value of  $R_0$  can be close to unity, provided the longevity of state 2. However, non-thermalization within the dark sector typically requires small values of the dark coupling  $g_V \lesssim 10^{-3.5} \sqrt{m/\text{MeV}} (m_V/m)^{1/4}$  as obtained from considering the rate for  $VV \leftrightarrow 11$  (22). In this case, the corresponding condition to achieve  $R_0 = O(1)$  is the same as Eq. (3.10), but the temperature ratio between two sectors now relies on the details of freeze-in. Roughly, the upper limit on  $g_V$  for freeze-in can be approximated by setting  $T'_{\text{FO}} \sim T_{\text{FO}} \sim m$  in Eq. (3.10), suggesting quite small dark couplings  $g_V \lesssim 10^{-3.5} m_V/(m \Delta m \text{ MeV}^2)^{1/4}$ . Therefore, for both 4-to-2 SIMP annihilation and freeze-in,  $R_0 \simeq 1$  cannot be achieved for sizable large dark couplings, unless new ingredients such as dark radiation or non-standard cosmology are considered.

## 4 Astrophysical Implications of Split SIMPs

So far we have studied how the DM relic abundance can be generated in the early Universe for split SIMPs and computed the relative abundance of the two states. The assumed small mass splitting and the feeble coupling to the SM sector suppress the decay width of the heavier state, making a two-component DM model viable. In this section we investigate the ensuing astrophysical implications.

Due to the non-diagonal coupling in the dark sector, self-scattering  $11 \rightarrow 11$  only appears at the loop-level. Hence, the relative abundance of states 1 and 2,  $R_0$ , enters in the DM self-scattering  $12 \rightarrow 12$  in dark halos of dwarf galaxies and colliding clusters as well as in the determination of the free-streaming length of keV DM affecting structure formation. Even if state 2 decays, it may affect structure formation at small scales due to the small velocity kick that the daughter DM particle receives. These three effects are investigated separately below, and the results are summarized in Fig. 5 for  $\Delta m/m = 10^{-2}$  (left panel) and  $10^{-6}$  (right panel). While they are calculated for pseudo-Dirac DM, similar results apply to scalar DM.

### 4.1 Decaying DM after Decoupling

The ratio of states 2 and 1 today,  $R_0$ , is obtained from the value of decoupling by  $R_0 = R_{\text{dec}} e^{-t_0/\tau_2} \sim R_{\text{dec}} e^{-\Gamma_2/H_0}$  where  $\tau_2 = \Gamma_2^{-1}$  is the lifetime of state 2. In the minimal set-up, decays into a single on-shell photon final state,  $\phi_2 \rightarrow \phi_1 \gamma$  and  $\chi_2 \rightarrow \chi_1 \gamma$ , cannot occur through kinetic mixing.<sup>6</sup> State 2 hence decays to state 1 plus a pair of SM fermions, or three photons, depending on kinematics. The decay into an electron/positron pair  $\chi_2 \rightarrow \chi_1 V^* \rightarrow \chi_1 e^+ e^-$  is allowed for  $\Delta m > 2m_e$  and typically dominates the total decay rate. For kinematically unsuppressed decay,

$$\Gamma_{\chi_2 \rightarrow \chi_1 e^+ e^-} \simeq \frac{2\alpha \alpha_V \kappa^2}{15\pi} \frac{\Delta m^5}{m_V^4} \simeq 2 H_0 \times \frac{m}{100 \text{ MeV}} \frac{\alpha_V}{\alpha} \left( \frac{\kappa}{10^{-10}} \right)^2 \left( \frac{\Delta m/m}{10^{-3}} \right)^5 \left( \frac{m}{m_V} \right)^4, \quad (4.1)$$

where  $H_0$  is the Hubble constant, implying a lifetime that can be comparable to the age of the Universe. For scalar DM an extra factor of 2 needs to be added. The total decay width to SM neutrinos,  $\Gamma_{\chi_2 \rightarrow \chi_1 \nu \bar{\nu}}$ , is suppressed by another factor of  $(m_V/m_Z)^4 \times 3/(8 \cos^4 \theta_W)$ .<sup>7</sup> If

<sup>6</sup>This can be seen from partial integration of  $V_{\mu\nu} F_Y^{\mu\nu} = -2V_\nu \partial_\mu F_Y^{\mu\nu} = 0$  setting the photon on-shell. Anomalous operators ( $VFF$ ,  $VVF$ ) are also negligible since the dark sector is non-chiral up to the mixing with the  $Z$  boson.

<sup>7</sup>A faster rate into neutrinos is possible if, in addition to kinetic mixing,  $V$  and  $Z$  mix through their mass terms,  $\Gamma_{V \rightarrow \nu \bar{\nu}} \propto \delta_Z^2 m_V^3/m_Z^2$  where  $\delta_Z \ll 1$  is a dimensionless number parametrizing the mixing [69].

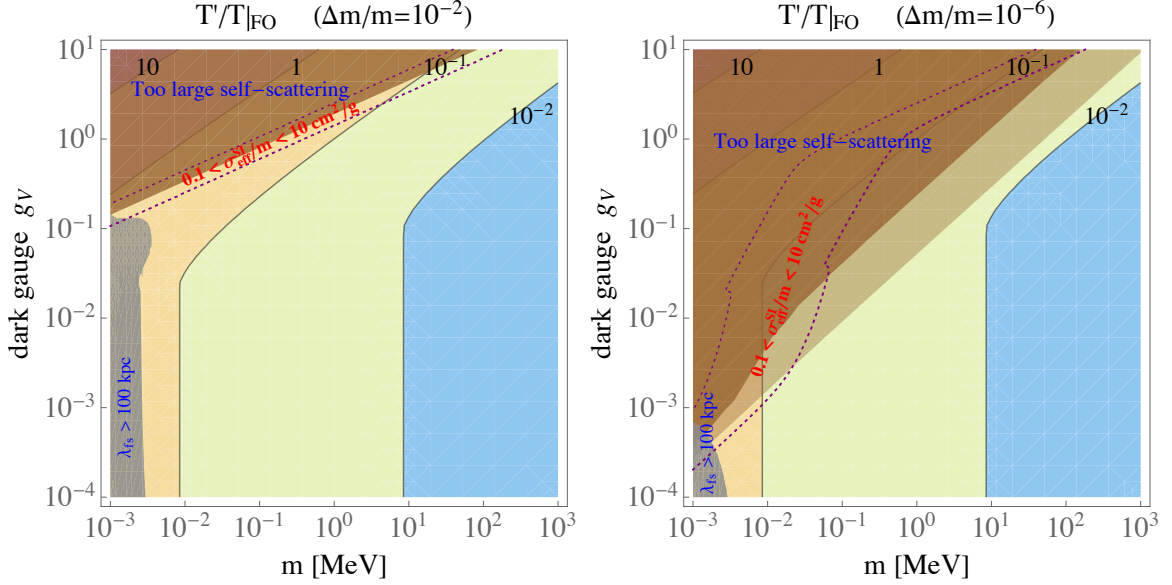


**Figure 5.** Pseudo-Dirac DM assuming  $m_V = \frac{5}{2}m$  and  $\Delta m/m = 10^{-2}$  (left) and  $10^{-6}$  (right). Contours show the temperature ratio of dark sector to visible sector at 4-to-2 freeze-out; current constraints are shown by shaded regions, labeled in blue. In the dark (light) brown shaded region the *effective* self-scattering cross section per DM mass is larger than  $1 \text{ cm}^2/\text{g}$  assuming  $v_0 = 250 \text{ km/s}$  ( $v_0 = 1000 \text{ km/s}$ ). In addition, the window between  $\sigma_{\text{eff}}^{\text{SI}}/m = 0.1 \text{ cm}^2/\text{g}$  and  $10 \text{ cm}^2/\text{g}$  for dwarf galaxies ( $v_0 = 30 \text{ km/s}$ ) is bounded by the dotted lines. Inside this region, small-scale structure problems can be addressed by DM.

the decay to charged lepton pairs is kinematically forbidden, the decay proceeds dominantly via the emission of three photons,  $\chi_2 \rightarrow \chi_1 V^* \rightarrow \chi_1 3\gamma$ ,

$$\begin{aligned} \Gamma_{\chi_2 \rightarrow \chi_1 3\gamma} &\simeq \Gamma_{\chi_2 \rightarrow \chi_1 \nu \bar{\nu}} \times \frac{\Gamma_{V \rightarrow 3\gamma}}{\Gamma_{V \rightarrow \nu \bar{\nu}}} \bigg|_{m_V \rightarrow \Delta m} \\ &\simeq H_0 \times \left( \frac{m}{50 \text{ MeV}} \right)^9 \frac{\alpha_V}{\alpha} \left( \frac{\kappa}{10^{-10}} \right)^2 \left( \frac{\Delta m/m}{10^{-2}} \right)^{13} \left( \frac{m}{m_V} \right)^4. \end{aligned} \quad (4.2)$$

where we have made use of the expression for  $\Gamma_{V \rightarrow 3\gamma}$  as given in Ref. [70] in the second line. Owing to the strong dependence  $\Delta m/m$  it shows that for  $\Delta m < 2m_e$  state 2 quickly becomes extremely long-lived. Hence, it is always possible to realize  $R_0 \simeq R_{\text{dec}}$  and we conclude that the model typically features two-component DM where state 2 decays on cosmological time scales.

Decaying DM has long been proposed as a solution to small scale structure problems. For instance, the cosmological simulation in Ref. [71] has suggested that if the lifetime of a heavier state is of the order of the age of the Universe, the kick velocity  $v_k$  received by the daughter DM particle should be around 20–40 km/s, or  $(0.6 - 1.2) \times 10^{-4}c$ , to appreciably modify structure formation at comoving length scales of  $\mathcal{O}(100)$  kpc. The split SIMP provides a new example of this kind of models since  $v_k/c \simeq \Delta m/m$  pointing to the  $\Delta m/m = 10^{-4}$  ballpark. Finally, we note in passing that DM decay into radiation, without seriously disrupting halo-structure (non-relativistic kick), is not able to reduce the discrepancy between *Planck* and low-redshift measurements of  $H_0$  [72]. To address the last discrepancy, both  $R_0 \sim 1$  and  $\Delta m/m \sim 0.1$  are required.

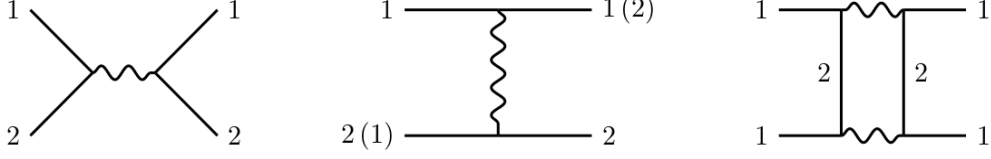


**Figure 6.** Main processes contributing to DM self-scattering involving an initial state 1. The first two diagrams contribute to the scattering between two different states,  $12 \rightarrow 12$ . The middle diagram can also contribute to inelastic up-scattering,  $11 \rightarrow 22$  and the last diagram shows the radiatively induced scattering  $11 \rightarrow 11$ .

## 4.2 Self-scattering of SIMPs

After having established the conditions for longevity of the excited state above, we now turn to its implications in the low-redshift Universe. Figure 6 shows the contributions to the self-scattering involving an initial state 1.<sup>8</sup> They are  $12 \rightarrow 12$  elastic scatterings,  $11 \rightarrow 22$  endothermal scatterings and radiatively induced  $11 \rightarrow 11$  scatterings denoted as  $\sigma_{12}$ ,  $\sigma_{\text{en}}$  and  $\sigma_{\text{rad}}$ , respectively.<sup>9</sup> The cross sections for these processes are listed in Appendix C for both fermionic and bosonic DM.

As explained in Sec. 1, a SIMP model that is able to address small-scale structure problems should have a self-interaction cross section of  $\sigma/m \geq 0.1 \text{ cm}^2/\text{g}$  inside dwarf galaxies. In contrast, at larger scales astrophysical observations suggest an upper bound on DM self-interaction. Given the uncertainties existing in the relevant constraints [52, 74], as a simple criterion, we required the effective self-scattering cross section involving state 1 over DM mass, as defined below, to be smaller than  $1 \text{ cm}^2/\text{g}$  at the galactic scale,

$$\frac{\sigma_{\text{eff}}^{\text{SI}}}{m} \equiv R_0 \frac{\sigma_{12}}{m} + \frac{\langle \sigma_{\text{en}} v \rangle}{2m v} + \frac{\sigma_{\text{rad}}}{2m} \lesssim 1 \text{ cm}^2/\text{g}, \quad (4.3)$$

where a statistical factor of  $1/2$  has been added to avoid double-counting in the latter two terms. The first term includes a factor of  $R_0$  as the interaction rate for  $12 \rightarrow 12$  hinges on the abundance of states 2,  $\Gamma_{12} \simeq R_0 n_1 \langle \sigma_{12} v \rangle$ . If state 2 has decayed, the remaining tree-level contribution to self-scattering is given by the second term, describing the endothermic scattering  $11 \rightarrow 22$ . Here, the relative kinetic energy of initial particles with relative velocity  $v$  must bridge the mass splitting,

$$\langle \sigma_{\text{en}} v \rangle \equiv \sigma_{\text{en}}^0 \iint d^3 \vec{v}_{1,2} f_1^{\text{MB}} f_2^{\text{MB}} \sqrt{1 - \frac{2\Delta m}{mv^2}} |v| \simeq \sqrt{\frac{2}{\pi}} \sigma_{\text{en}}^0 v_0 \left[ \xi e^{-\xi} K_1(\xi) \Theta \left( v_{\text{esc}} - v_0 \sqrt{\xi} \right) \right], \quad (4.4)$$

where  $v_{\text{esc}}$  is the escape velocity and  $v_0$  is related to the velocity dispersion of the system,  $v_0 = \sqrt{2}\sigma$ ;  $f_i^{\text{MB}} = N e^{-\vec{v}_i^2/v_0^2}$ , normalized to unity. The Heaviside step function  $\Theta$  provides the kinetic cutoff for up-scattering. Here  $K_1(\xi)$  is the Bessel function of the second kind, with  $\xi \equiv 2\Delta m/(mv_0^2)$ ; hence, the last factor in the square bracket converges to 1 for  $\xi \rightarrow 0$ , and becomes exponentially suppressed for  $\xi \gg 1$ . The third term in Eq. (4.3) accounts for the radiatively induced elastic scattering  $11 \rightarrow 11$ . It is dominated by diagrams with the exchange of two (heavy)  $V$  bosons, and has an interaction rate  $\Gamma_{\text{rad}} = n_1 \langle \sigma_{\text{rad}} v \rangle$ . This process can be

<sup>8</sup>The rate for self-scattering of states 2,  $22 \rightarrow 11$  or  $22 \rightarrow 22$ , is suppressed by  $R_0^2$  and correspondingly less important.

<sup>9</sup>The case of self-interacting inelastic DM where self-scatterings take place through light mediators has been studied in Ref. [73].

important for certain parameter regions where a large mass splitting significantly reduces the contributions of the two previous contributions.

In Fig. 4, we identify the region in the  $[g_V, m]$  plane which yields  $R_0 \sigma_{12}/m = 1 \text{ cm}^2/\text{g}$  by the dashed lines at the top-left corners. The left (right) panel corresponds to  $\Delta m/m = 10^{-2}$  ( $10^{-6}$ ). The value of  $R_0$  is computed from the decoupling and  $R_0 = R_{\text{dec}}$  has been assumed. As a comparison, parameters associated with  $\sigma_{12}/m = 1 \text{ cm}^2/\text{g}$  are also given by the dotted line in each panel, highlighting the importance of tracking  $R$  until the decoupling of the 2-to-2 process in the early Universe. The potentially excluded regions from self-scattering,  $\sigma_{\text{eff}}^{\text{SI}}/m > 1 \text{ cm}^2/\text{g}$  at the galactic scale (at the cluster scale) are given by the dark (light) brown shaded regions in both panels of Fig. 5. For the left panel, both exclusions coincide because the endothermic channel is always strongly suppressed due to the large mass splitting. Meanwhile,  $\sigma_{\text{eff}}^{\text{SI}}/m = 0.1 \text{ cm}^2/\text{g}$  and  $10 \text{ cm}^2/\text{g}$  for dwarf galaxies are shown with two dotted lines; the region in between addresses the aforementioned small-scale structure problems.

It is worth emphasizing that the constraint (4.3) has to be viewed with some caution. The abundance ratio of the two species is assumed to be universal, and is set to be  $R_0$ . In practice, this ratio may depend on the dynamics and merger history of dark halos. On the one hand, dense DM halos with large velocity dispersion may enhance the  $11 \rightarrow 22$  endothermic process, thereby increasing  $R_0$  differentially in those objects. On the other hand, as state 2 only contributes a small portion of the total DM abundance, scattering with state 1, during halo mergers, may deplete state 2 in the inner regions of halos, hence suppressing the overall effect of DM self-interactions. Accounting for the latter likely requires cosmological simulation and is beyond the scope of this work.

### 4.3 Free Streaming

Self-scattering is also relevant in the high-redshift Universe as it controls the free-streaming of DM particles, which in turn determines the smallest DM objects that can be formed from primordial perturbations [75]. Here, two competing effects need to be considered. First, in the 4-to-2 annihilation process, DM particles get boosted in the final state. The dark sector hence has a tendency to be naturally hotter than the SM after freeze-out, adding to the free-streaming after DM chemical decoupling. Second, 2-to-2 self-scattering will keep the particles contained up to diffusive processes until a temperature  $T'_k$  when the latter cease,

$$\Gamma_1(T'_k) \sim H(T_k) \quad (4.5)$$

where  $\Gamma_1 = n_1 \langle \sigma_{\text{eff}}^{\text{SI}} v \rangle$  for state 1. Apparently, this happens after the decoupling of the annihilation process  $22 \rightarrow 11$ , that is,  $T_k < T_{\text{dec}}$ . Since the interactions are short-range,  $m_V > m_1 + m_2$ , we are allowed to neglect the detailed momentum transfer in each collision [76].

After the DM kinetic decoupling at cosmic time  $t_k$ , the (non-relativistic) DM velocity redshifts as  $v_\chi(T') = (T/T_k) v_\chi(T'_k)$ , where  $v_\chi(T'_k) \simeq \sqrt{2T'_k/m}$ . The comoving free-streaming length  $\lambda_{\text{fs}}$  is given by integrating the velocity until matter-radiation equality at cosmic time  $t_{\text{eq}}$ ,

$$\lambda_{\text{fs}} = \int_{t_k}^{t_{\text{eq}}} \frac{v_\chi(t)}{a(t)} dt \sim \frac{26 \text{ kpc}}{\sqrt{g_\star(T_k)}} \times \frac{10 \text{ keV}}{\sqrt{T_k m}} \left( \frac{T'_k}{T_k} \right)^{1/2} \log_{10} \left( \frac{T_k}{T_{\text{eq}}} \right). \quad (4.6)$$

Here, we assumed that the Hubble rate  $H$  is dominated by the SM energy density and  $g_\star(T)$  counts the SM relativistic degrees of freedom at photon temperature  $T$ ;  $T_0$  and  $T_{\text{eq}}$  are the corresponding temperatures at present and at matter-radiation equality, respectively. In our



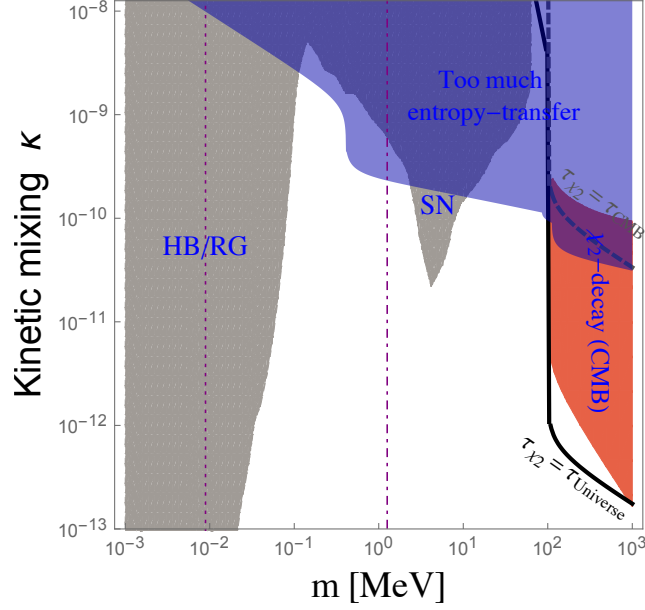


**Figure 7.** Bounds on the kinetic mixing parameter  $\kappa$  for  $\Delta m/m = 10^{-2}$  and  $g_V = e$  for pseudo-Dirac DM. The mass of  $V$  is set to be  $\frac{5}{2}m$ . To the right of the solid (dashed) thick contour lines the lifetime of state 2 falls below the age of the Universe (the cosmic time at last scattering). All shaded regions with labels in blue are excluded (see text for details.) The two thin vertical lines show DM self-interaction bounds for  $\Delta m/m = 10^{-2}$  (dotted) and  $10^{-6}$  (dash-dotted), respectively. The corresponding regions to the left are disfavored.

numerical evaluation, we additionally take into account the free-streaming in the matter-dominated epoch.

The strongest observationally inferred limit on  $\lambda_{\text{fs}}$  is derived from the matter power spectrum suppression induced by DM free-streaming and comparing Lyman- $\alpha$  observations and cosmological hydrodynamical simulations. The current limit is  $\lambda_{\text{fs}} \lesssim 100$  kpc [77, 78] and it is shown by the gray shaded region in Fig. 5. As can be seen, the bound for sizable  $g_V$  is very weak due to the efficient DM self-scattering. Finally, we point out that there are additional effects from collisional damping and dark acoustic oscillations [79], which are not considered here because they only lead to a suppression of the matter power spectrum at similar or scales smaller than  $\lambda_{\text{fs}}$  for our parameter choices. They become important in the limit  $m_V \ll m$  for which additional dark radiation in form of  $V$  remains coupled with DM [80].

## 5 Sensitivity and Constraints on the Kinetic Mixing Portal

By assumption, the dark sector interacts with the SM through the “kinetic mixing” portal. The requirement on maintaining decoupled sectors in the early Universe, and on ensuring longevity of state 2, implies  $\kappa \ll 10^{-6}$ , precluding missing energy searches in both collider and fixed-target experiments. Although astrophysics remains the best probe, indirect and direct searches have some potential to probe the model by exploiting the mass splitting between the two states. Below we provide a brief discussion thereof, and for exemplary mass-splitting  $\Delta m/m = 10^{-2}$  and  $g_V = e$ , the parameter space in  $[m, \kappa]$  is chartered out in Fig. 7.



- Equation (3.4) relates the relative comoving entropies of the hidden and SM sector,  $S'/S \ll 1$ , through the DM relic abundance requirement. A priori, this ratio can be originated from sources independent of the SM, such as a branching of the inflaton decaying into the dark sector. Any finite value of  $\kappa$  will lead to the transfer of energy/entropy from the SM to the dark sector, hence increasing the ratio  $S'/S$  and thereby imposing an upper limit on the strength of the portal interaction. Notice that the energy transfer is significantly enhanced if  $V$  bosons can be created on-shell by electron pair annihilation, *i.e.*,  $m_V \geq 2m_e$ . This implies  $\kappa \lesssim \mathcal{O}(10^{-10})$  for MeV DM with a heavier  $m_V$  and no additional contributions to the DM abundance. In turn, for  $m_V < 2m_e$  the value of  $\kappa$  is allowed to increase into observationally more interesting regimes. The excluded region assuming no other a priori sources than SM for dark sector particles is labeled “too much entropy-transfer” in Fig. 7.
- The decay of state 2 into state 1 is accompanied by SM radiation, injecting an energy per baryon of  $E_{\text{inj}}/n_B = \Delta m (R_{\text{dec}} n_1)/n_B$ , possibly constrained by BBN and CMB. For BBN, the ballpark of sensitivity on electromagnetic energy injection is  $\mathcal{O}(\text{MeV})/\text{baryon}$  for  $\tau_2 \gtrsim 10^5 \text{ s}$ , see *e.g.* Ref. [81]. Hence, only mass-splittings  $\Delta m \gtrsim \text{MeV} > 2m_e$  are energetically relevant, where the decay proceeds by producing an electron-positron pair. We conclude that, approximately,

$$\frac{\Delta m}{m} \lesssim \frac{10^{-3}}{5R_{\text{dec}} \text{Br}_{\text{em}} e^{-t/\tau_2}} \quad (5.1)$$

should hold for respecting the limits on electromagnetic energy injection (with branching  $\text{Br}_{\text{em}}$ ) from BBN; the factor 5 is the ratio  $\Omega_{\text{DM}}/\Omega_b$  of DM to baryon densities today, assuming that decoupling in the dark sector happens before  $t \sim 10^5 \text{ s}$ . It turns out that in our model the BBN constraints are respected. Longer lifetimes are most stringently constrained by CMB measurements [1, 82, 83], rather than by indirect searches [84]. The limits derived in Ref. [83] can be cast into

$$\frac{\Delta m}{m} \lesssim \frac{\tau_2}{10^{24} \text{ s}} \frac{1}{\text{Br}_{\text{em}} R_{\text{dec}}}, \quad (5.2)$$

which is shown as the orange shaded region on the right-hand side of Fig. 7. As can be seen from the figure, when the channel to electrons becomes kinetically forbidden at  $m \lesssim 100 \text{ MeV}$ ,  $\tau_2$  increases dramatically and surpasses this bound.

- The heavier state behaves as exothermic DM and may thus be detectable in direct detection experiments. Although its mass lies below the GeV scale, the energy transfer to the target  $A$  (nucleus or electron) through the inelastic collision  $2 + A \rightarrow 1 + A$ ,

$$E_{\text{recoil}} \sim \Delta m \frac{\mu_{mA}}{m_A}, \quad (5.3)$$

where  $\mu_{mA}$  is the reduced mass between DM and target, can be larger than the experimental threshold. The scattering results in a monochromatic signal, up to corrections proportional to the relative kinetic energy and bound state effects (the latter of which can be substantial). For the small mass splittings of interest, collisions with electrons are more prospective, as they cause larger energy transfer. The cross section on the latter is given by

$$\bar{\sigma}_e \simeq a 10^{-44} \text{ cm}^2 \times \frac{\alpha_V}{\alpha} \left( \frac{\kappa}{10^{-10}} \right)^2 \left( \frac{m}{100 \text{ keV}} \right)^2 \left( \frac{300 \text{ keV}}{m_V} \right)^4, \quad (5.4)$$

where  $a = 1$  ( $1/2$ ) for fermions (scalars) and assuming  $m \lesssim m_e$ . Since we consider  $m_V > 2m$ , the cross section is suppressed and current sensitivity from ionization only data from XENON10 [85] and XENON100 [86] falls short; DM limits based on the latter data for elastic scattering and absorption have previously been presented in Refs. [87–90]. However, once  $\Delta m \gtrsim 1$  keV the energy deposition is large enough for reducing the background via the scintillation signal. Adopting the results from an axion search in XENON100 [91] we find that direct detection starts probing the plane for  $\sqrt{R_0} \kappa \gtrsim 10^{-9}$  with improvements expected from LUX [92] and XENON1T [93]. Finally, a whole number of proposed searches may be able to improve the sensitivity on  $\kappa$ —and to be sensitive to minute  $\Delta m \lesssim$  eV—in the future [94–99]; see Appendix D for details on the derivation and more results of the direct detection region.

- Finally, astrophysical constraints are of significant relevance at probing the production and emission of feebly interacting light particles from stars, such as horizontal branch (HB) and red giants (RG), as well as supernovae (SN) [100]. For  $m \lesssim 100$  keV, energy losses from stars by on-shell production of  $V$  dominate the constraints on  $\kappa$ , see Refs. [88, 101, 102]. MeV-scale DM is constrained by SN where we adopt the latest bound from Refs. [103, 104]. The astrophysically disfavored regions are shown by the gray shaded regions as labeled. Note that in our scenario  $V$  decays promptly and dominantly into lighter dark particles in contrast to (meta-)stable  $V$ -bosons considered in Refs. [68, 84].

Most of the parameter space shown in Fig. 7 corresponds to a state 2 with a lifetime that exceeds the age of the Universe. Only in the small region delimited by the solid black line in the top-right corner, the heavy state effectively decays. As discussed in the previous section, the abundance of state 2 plays an important role in addressing small-scale problems if  $\sigma_{12}/m$  is large. All shown constraints can be easily rescaled to values of  $g_V$  from  $\sim 10^{-4}$  to  $\mathcal{O}(1)$ . The bounds from stars (HB and RG) as well as from SN (gray shaded region) are independent of  $g_V$ ; for as long as  $V$  decays dominantly within the dark sector, the lifetime of  $V$  does not enter the energy loss argument. The constraint on entropy-transfer (blue shaded region) is derived under the conservative condition that the dark sector becomes populated only through the portal interaction. The value of  $g_V$  is only relevant when  $m_V \lesssim 1$  MeV and  $g_V \gtrsim e$ , as otherwise the on-shell production of vectors  $V$  dominates the entropy-transfer. For bounds from indirect (and future direct) searches, one has to take into account the corresponding change of  $R_0$ ; smaller values weaken the constraints on  $\kappa$ . Since  $R_0 \propto g_V^{-4}$ , obtained from Eq. (3.9), the y-axis can be replaced by  $(e/g_V) \kappa$ . Finally, the limits on self-scattering are not easily rescaled with  $g_V$  but are shown as two vertical purple lines for  $\Delta m/m = 10^{-2}$  (dotted) and  $10^{-6}$  (dash-dotted). For each mass splitting value and  $g_V = e$ , parameter region on the left side of the line has been excluded. Such limit on  $m$  weakens with the decrease of  $g_V$ .

## 6 Conclusions and Outlook

In this paper we have considered a variant of strongly (yet perturbatively) self-interacting DM models in which scattering rates are controlled by a fine mass splitting  $\Delta m/m$  between an otherwise degenerate pair of real scalars  $\phi_{1,2}$  or Majorana fermions  $\chi_{1,2}$ . The gauged dark U(1) symmetry with vector  $V$  and gauge coupling  $g_V$  is explicitly broken by  $\Delta m$  and thus the interaction with DM proceeds off-diagonally.

We first calculate the DM relic abundance in 4-to-2 number-depleting processes. It is well known that the requirement for successful 3-to-2 or 4-to-2 freeze-out points towards sub-GeV

DM, and we study the principal DM mass range from keV to GeV. In order to avoid constraints on dark radiation during BBN, we consider a scenario in which the dark and observable sector do not reach thermal equilibrium. Non-relativistic four-fermion annihilation is inhibited by the Pauli exclusion principle and requires two spin-singlet pairs of  $2\chi_1$  and  $2\chi_2$ . The efficiency of annihilation is hence regulated by the number ratio  $R = n_2/n_1 \sim e^{-\Delta m/T'}$ , which, in turn puts a requirement on the minimum value of  $g_V$  for given  $\Delta m$  and given ratio of photon and dark sector temperatures at freeze-out  $T'/T|_{\text{FO}}$ . In contrast, for scalars, we find the required value of  $g_V$  to be largely independent of  $\Delta m$  as  $4\phi_1$  annihilation channels are open.

We then track the ratio  $R$  until it is frozen out in the decoupling of the  $12 \leftrightarrow 12$  process. This sets the boundary condition for the self-scattering in DM halos today: whereas the  $11 \rightarrow 22$  (11) scattering is kinematically (radiatively) suppressed, the scattering  $12 \rightarrow 12$  is regulated by the value of  $R_0$  in the low redshift Universe. The latter is determined by the lifetime of state 2,  $\tau_2$ , through  $R_0 = R_{\text{dec}} e^{-t_0/\tau_2}$ . We choose a kinematic setting  $m_V \geq 2m + \Delta m$  so that  $V$  decays promptly within the dark sector;  $\tau_2$  is then determined by the off-shell decay  $2 \rightarrow 1 + V^* \rightarrow 1 + \text{SM}$ . For this we couple  $V$  to SM through kinetic mixing with strength  $\kappa$ , and for  $\Delta m \leq 2m_e$  state 2 becomes quickly stable on cosmological timescales.

Since freeze-out in the dark sector through number-violating processes can lead to hot DM, it is usually surmised that the coupling to SM must bring DM into kinetic equilibrium with SM, putting a lower bound on  $\kappa$ . Here, we study an alternative scenario in which the dark sector remains decoupled from SM, but free-streaming constraints are respected 1) by the containment of particles through self-scattering (with diffusion playing a sub-leading role) and 2) by a freedom of choice in the initial temperature ratio  $T'/T$  of both sectors.

Astrophysical bounds on the scenario are controlled by  $\kappa$  as it regulates the emission of light DM states through the production of  $V$  and the allowed parameter space is identical to the one for long-lived “dark photons”. We identify the parameter regions where the relic density requirement is matched, and where, at the same time, a self-scattering cross section of  $0.1 \lesssim \sigma/m \lesssim 10 \text{ cm}^2/\text{g}$  is attained. The latter ballpark is proposed to solve the small-scale problems in the collisionless DM paradigm. We find that it is possible to reach such regions in parameter space while respecting all astrophysical and cosmological constraints.

In a final step, we study the detectability of the scenario in terrestrial experiments. The requirement that dark and observable sectors remain decoupled in the early Universe, puts collider probes out of reach. However, the exothermic  $2 \rightarrow 1$  scattering on electrons leads to a quasi-monochromatic energy deposition, enhancing the prospects in direct detection experiments. We find that provided that  $\Delta m > 1 \text{ keV}$  and  $R_0 \sim 1$ , the scenario is on the verge of being probable with reported data (S1 and S2) from XENON100, despite the requirement  $\kappa \lesssim 10^{-9}$ . Ionization only (S2) studies are not sensitive at this point.

Several points raised in the paper prompt further investigation. First, we specialized to the case  $m_V > 2m + \Delta m$ , which is a restrictive requirement for both efficient annihilation, and detectability in underground rare event searches. It was largely motivated by evading constraints on extra radiation and from astrophysics, however, a more detailed exploration of the parameter space is certainly warranted, particularly in light of upcoming CMB measurements with much improved error bar on dark radiation,  $\sigma(N_{\text{eff}}) = O(10^{-2})$  [105, 106]. Second, as we have shown, future direct detection experiments will be sensitive to this physics, despite the requirement that dark and observable sector never reach thermal equilibrium and the above limit of a “heavy” mediator. Following recent proposals to employ semiconductor targets with sensitivity to  $O(\text{eV})$  energy depositions, among others, a more general study of exothermic DM scattering with astrophysically motivated mass splittings  $\Delta m/m = O(v^2) \sim 10^{-6}$  as well

as lighter mediators is certainly motivated. We leave such and related points for future work.

## Acknowledgments

NB thanks F. Staub and A. Vicente for helpful discussions. NB is partially supported by the São Paulo Research Foundation (FAPESP) under grants 2011/11973-4 & 2013/01792-8, the Spanish MINECO under Grant FPA2014-54459-P and by the “Joint Excellence in Science and Humanities” (JESH) program of the Austrian Academy of Sciences. XC and JP are supported by the “New Frontiers Program” by the Austrian Academy of Sciences. This project has received funding from the European Union’s Horizon 2020 research and innovation programme under the Marie Skłodowska-Curie grant agreements 674896 and 690575.

## A Annihilation Rates

Here we provide some details on the rates that go into the Boltzmann equation for the 4-to-2 process. The squared matrix elements  $|\overline{M}|^2$  are obtained in the usual way and, for fermions, are summed (averaged) over final (initial) state spins; a symmetry factor of 1/2 is included for identical final state particles. For reasons of a tractable exposition, we only list the leading order in relative velocities and  $\Delta m$ , which means a constant in both quantities. Therefore, the phase space integration is trivial, the squared matrix elements only depend on the initial state configuration, and the rates are directly obtained from the latter through,

$$\langle ijkl \rightarrow mn \rangle = \frac{S_{ijkl}}{m_i m_j m_k m_l} \frac{1}{32\pi} \frac{p_f}{\sqrt{s}} |\overline{M}_{ijkl}|^2, \quad (\text{A.1})$$

$$\simeq \frac{\sqrt{3} S_{ijkl}}{128\pi m^4} |\overline{M}_{ijkl}|^2. \quad (\text{A.2})$$

where  $p_f$  is the magnitude of the final state relative momentum and  $\sqrt{s}$  is the total incoming energy;  $S_{ijkl}$  is a statistical factor comprising a symmetry factor ( $1/n!$  for each set of  $n$  identical initial state particles) times the multiplicity of particles that are removed from the plasma in the annihilation (2 in this case). Detailed balancing allows to make contact with an actual 2-body cross section  $\langle \sigma_{mn} v \rangle$  of particles  $m$  and  $n$  in the 2-to-4 process

$$\langle ijkl \rightarrow mn \rangle = 2 \langle \sigma_{mn} v \rangle \frac{n_m^{\text{eq}} n_n^{\text{eq}}}{n_i^{\text{eq}} n_j^{\text{eq}} n_k^{\text{eq}} n_l^{\text{eq}}}, \quad (\text{A.3})$$

in which the prefactor of 2 gives the particle number changed by per reaction. In the case  $m = n$ , another factor 1/2 needs to be added to the RHS to avoid over-counting.

For pseudo-Dirac DM the only non-zero reactions for  $ijkl \rightarrow mn$  are  $2\chi_i + 2\chi_j \rightarrow 2\chi_i$  with  $i \neq j$ ,

$$|\overline{M}_{1122}|^2 \simeq 216 g_V^8 \frac{m^4 (m_V^4 - 8m^2 m_V^2 - 8m^4)^2}{(m_V^4 - 2m^2 m_V^2 - 8m^4)^4}; \quad (\text{A.4})$$

for scalars, we find

$$|\overline{M}_{ijkl}|^2 \simeq c_{ijkl} \frac{g_V^8 m^4}{(2m^2 + m_V^2)^4}. \quad (\text{A.5})$$

with  $c_{1122} = 72$ ,  $c_{1111} = c_{2222} = 5184$ ,  $c_{1112} = c_{1222} = 432$ . Equations (A.4) and (A.5) are exact in the limit  $\Delta m = 0$ , in the numerical analysis we have used however the full expressions. The sizable number of matrix elements were computed by implementing the models into `CalcHEP` [107] and `FeynArts` [108].

## B Solution to the Boltzmann Equation

At freeze-out, the DM density starts exceeding from its equilibrium value,  $Y \gg Y_{\text{eq}}$ , so that the term proportional to  $Y_{\text{eq}}$  can be dropped in Eq. (3.2) to obtain the yield of DM at present,

$$Y_0 \simeq \left[ \frac{1}{Y(x_{\text{FO}})^3} + 3 \int_{x_{\text{FO}}}^{\infty} \frac{s^3 \langle \sigma v^3 \rangle_{4 \rightarrow 2}}{x H} dx \right]^{-1/3} \simeq \left[ 3 \int_{x_{\text{FO}}}^{\infty} \frac{s^3 \langle \sigma v^3 \rangle_{4 \rightarrow 2}}{x H} dx \right]^{-1/3}, \quad (\text{B.1})$$

where  $Y_0 \ll Y(x_{\text{FO}})$  is also used in the last step. The observed relic density parameter today [1] reads,<sup>10</sup>

$$\Omega_{\text{DM}} = \frac{m s_0 Y_0}{\rho_c} = (2.742 \times 10^8 \text{ GeV}^{-1} h^{-2}) m Y_0, \quad (\text{B.2})$$

where  $s_0$  and  $\rho_c$  denote the respective SM entropy density and critical energy density today.

## C Decay Rates and Self-scattering Cross Sections

For DM self-scattering where state 2 has a lifetime much in excess of the age of the Universe, DM may self-scatter entirely elastically,  $12 \rightarrow 12$ , with cross section:

$$\text{Pseudo-Dirac: } \sigma_{12} = \frac{g_V^4 m^2}{4\pi m_V^4} \left[ \frac{16m^4 - 20m^2 m_V^2 + 7m_V^4}{(4m^2 - m_V^2)^2} \right], \quad (\text{C.1})$$

$$\text{Scalar: } \sigma_{12} = \frac{g_V^4}{4\pi} \frac{m^2}{m_V^4}. \quad (\text{C.2})$$

The cross section for the endothermic scattering  $11 \rightarrow 22$  is given by (neglecting contributions proportional to  $\delta^2$ )

$$\text{Pseudo-Dirac: } \sigma_{en} = \frac{g_V^4 m^2}{8\pi m_V^4} \sqrt{1 - \frac{2\Delta m}{mv^2}} \equiv \sigma_{en}^0 \sqrt{1 - \frac{2\Delta m}{mv^2}}, \quad (\text{C.3})$$

$$\text{Scalar: } \sigma_{en} = 4\sigma_{en}^0 \sqrt{1 - \frac{2\Delta m}{mv^2}}. \quad (\text{C.4})$$

The kinetic condition for the reaction is  $\Delta m < mv^2/2$ , where  $v$  is the DM velocity in the center-of-mass frame.

Radiatively induced elastic scattering  $11 \rightarrow 11$  can be important if the above two processes are both suppressed, either kinematically and/or by deficiency of reactant 2. From naive dimensional analysis one may estimate it as,

$$\sigma_{\text{rad}} \sim \frac{g_V^8 m^6}{256\pi^4 m_V^8}. \quad (\text{C.5})$$

Finally, for completeness, we also list the decay width of the heavy gauge boson,

$$\Gamma_{V \rightarrow \chi_1 \chi_2} = \frac{g_V^2 m_V}{12\pi} \left( 1 + \frac{\Delta m^2}{2m_V^2} \right) \left[ 1 - \frac{(2m + \Delta m)^2}{m_V^2} \right]^2. \quad (\text{C.6})$$

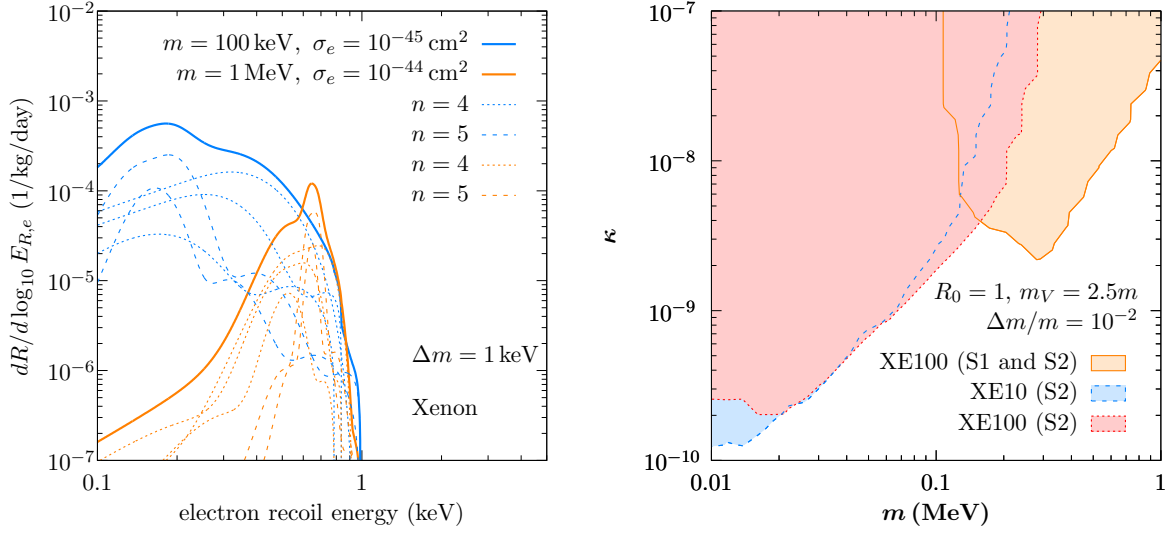


**Figure 8.** *Left:* Exothermic scattering on electrons and resulting recoil spectra in a liquid xenon detector for a 1 keV mass splitting and a combination of DM mass and scattering cross section (100 keV,  $10^{-45} \text{ cm}^2$ ) and (1 MeV,  $10^{-44} \text{ cm}^2$ ). *Right:* The parameter space of  $\kappa$  vs.  $m$  with current sensitivity in direct detection using the same choice of parameters as in Fig. 7 but equipartitioning the abundance of state 2,  $R_0 = 1$ .

## D Exothermic DM-Electron Scattering

Here we provide the formulæ for the exothermic scattering of state 2 to 1 on electrons, applicable to direct detection studies. A bound electron has a fixed energy  $E_e = m_e - E_B$  with  $E_B > 0$  being the magnitude of the binding energy, but a continuous distribution of momenta  $\vec{p}_e$ . The process we are considering is ionization, where the final state electron has kinetic recoil energy  $E_{R,e}$ . When  $\Delta m$  is larger than the typical kinetic energy of DM, the signal will correspond to a mono-chromatic energy deposition, with differential cross section,

$$\frac{d\sigma v}{d \ln E_{R,e}} = \bar{\sigma}_e \frac{m}{4\mu_{\chi e}^2} \times \left[ \int d\Omega_{\vec{p}_e} q |F_{\text{DM}}(q)|^2 \sum_{\text{deg. states}} |f_{\text{ion}}(q)|^2 \right]_{q=\sqrt{2m(\Delta m - E_B - E_{R,e})}} \quad (\text{D.1})$$

where  $q = |\vec{q}|$  is the magnitude of the transferred three-momentum  $\vec{q} = \vec{p}_2 - \vec{p}_1$ , *i.e.*, the difference in DM momenta of the respective states 2 and 1. Here,  $F_{\text{DM}}(q)$  and  $f_{\text{ion}}(q)$  are dimensionless form factors following the notation of Refs. [87, 109]. Our kinematic setup implies contact interactions with the electron,  $m_V \gg q$ , and the free DM-electron scattering cross section is given by,

$$\bar{\sigma}_e = a \frac{16\pi \alpha \alpha_V \kappa^2 \mu_{\chi e}^2}{m_V^4} \simeq 10^{-44} \text{ cm}^2 a \frac{\alpha_V}{\alpha} \left( \frac{\kappa}{10^{-10}} \right)^2 \left( \frac{m}{100 \text{ keV}} \right)^2 \left( \frac{300 \text{ keV}}{m_V} \right)^4, \quad (\text{D.2})$$

where  $a = 1$  (1/2) for fermions (scalars), and assuming  $m \lesssim m_e$  in the second equality.

For liquid scintillator detectors, the process is to a good approximation described by ionization from an isolated atom from a shell with principal and angular quantum number  $n$

<sup>10</sup>Assuming that the state 2 decays into 1 after the DM freeze out, with small correction proportional to  $\Delta m/m$  when state 2 is stable.

and  $l$ . The atomic form factor is then readily evaluated as the Fourier transform  $\chi_{nl}$  of the respective radial bound state wave function,

$$\frac{d\sigma_{nl} v}{d \ln E_{R,e}} = \bar{\sigma}_e \frac{(2l+1) m p_e'^2}{4 (2\pi)^3 \mu_{\chi e}^2} \int_{|p_e' - \sqrt{2m(\Delta m - E_B - E_{R,e})}|}^{p_e' + \sqrt{2m(\Delta m - E_B - E_{R,e})}} dp' p' |\chi_{nl}(p')|^2. \quad (\text{D.3})$$

Ensuing exemplary recoil spectra are shown in the left panel of Fig. 8. The right panel shows the parameter space of  $\kappa$  vs.  $m$  with current sensitivity in direct detection using the same choice of parameters as in Fig. 7 but equipartitioning the abundance of state 2,  $R_0 = 1$ . The statistical procedure for setting the limits follows the one outlined in Ref. [90]; see also Refs. [87–89].

## References

- [1] PLANCK collaboration, P. A. R. Ade et al., *Planck 2015 results. XIII. Cosmological parameters*, *Astron. Astrophys.* **594** (2016) A13, [[1502.01589](#)].
- [2] A. D. Dolgov, *ON CONCENTRATION OF RELICT THETA PARTICLES. (IN RUSSIAN)*, *Yad. Fiz.* **31** (1980) 1522–1528.
- [3] E. D. Carlson, M. E. Machacek and L. J. Hall, *Self-interacting dark matter*, *Astrophys.J.* **398** (1992) 43–52.
- [4] Y. Hochberg, E. Kuflik, T. Volansky and J. G. Wacker, *Mechanism for Thermal Relic Dark Matter of Strongly Interacting Massive Particles*, *Phys.Rev.Lett.* **113** (2014) 171301, [[1402.5143](#)].
- [5] N. Yamanaka, S. Fujibayashi, S. Gongyo and H. Iida, *Dark matter in the hidden gauge theory*, [1411.2172](#).
- [6] Y. Hochberg, E. Kuflik, H. Murayama, T. Volansky and J. G. Wacker, *Model for Thermal Relic Dark Matter of Strongly Interacting Massive Particles*, *Phys. Rev. Lett.* **115** (2015) 021301, [[1411.3727](#)].
- [7] N. Bernal, C. Garcia-Cely and R. Rosenfeld, *WIMP and SIMP Dark Matter from the Spontaneous Breaking of a Global Group*, *JCAP* **1504** (2015) 012, [[1501.01973](#)].
- [8] N. Bernal, C. Garcia-Cely and R. Rosenfeld,  $\mathbb{Z}_3$  WIMP and SIMP Dark Matter from a Global  $U(1)$  Breaking, *Nucl. Part. Phys. Proc.* **267–269** (2015) 353–355.
- [9] H. M. Lee and M.-S. Seo, *Communication with SIMP dark mesons via  $Z'$ -portal*, *Phys. Lett.* **B748** (2015) 316–322, [[1504.00745](#)].
- [10] S.-M. Choi and H. M. Lee, *SIMP dark matter with gauged  $\mathbb{Z}_3$  symmetry*, *JHEP* **09** (2015) 063, [[1505.00960](#)].
- [11] M. Hansen, K. Langæble and F. Sannino, *SIMP model at NNLO in chiral perturbation theory*, *Phys. Rev.* **D92** (2015) 075036, [[1507.01590](#)].
- [12] N. Bernal, X. Chu, C. Garcia-Cely, T. Hambye and B. Zaldivar, *Production Regimes for Self-Interacting Dark Matter*, *JCAP* **1603** (2016) 018, [[1510.08063](#)].
- [13] E. Kuflik, M. Perelstein, N. R.-L. Lorier and Y.-D. Tsai, *Elastically Decoupling Dark Matter*, *Phys. Rev. Lett.* **116** (2016) 221302, [[1512.04545](#)].
- [14] Y. Hochberg, E. Kuflik and H. Murayama, *SIMP Spectroscopy*, *JHEP* **05** (2016) 090, [[1512.07917](#)].
- [15] S.-M. Choi and H. M. Lee, *Resonant SIMP dark matter*, *Phys. Lett.* **B758** (2016) 47–53, [[1601.03566](#)].



- [16] D. Pappadopulo, J. T. Ruderman and G. Trevisan, *Dark matter freeze-out in a nonrelativistic sector*, *Phys. Rev.* **D94** (2016) 035005, [[1602.04219](#)].
- [17] M. Farina, D. Pappadopulo, J. T. Ruderman and G. Trevisan, *Phases of Cannibal Dark Matter*, *JHEP* **12** (2016) 039, [[1607.03108](#)].
- [18] S.-M. Choi, Y.-J. Kang and H. M. Lee, *On thermal production of self-interacting dark matter*, *JHEP* **12** (2016) 099, [[1610.04748](#)].
- [19] U. K. Dey, T. N. Maity and T. S. Ray, *Light Dark Matter through Assisted Annihilation*, [1612.09074](#).
- [20] N. Bernal and X. Chu,  $\mathbb{Z}_2$  SIMP Dark Matter, *JCAP* **1601** (2016) 006, [[1510.08527](#)].
- [21] A. A. de Laix, R. J. Scherrer and R. K. Schaefer, *Constraints of selfinteracting dark matter*, *Astrophys. J.* **452** (1995) 495, [[astro-ph/9502087](#)].
- [22] M. Heikinheimo, T. Tenkanen, K. Tuominen and V. Vaskonen, *Observational Constraints on Decoupled Hidden Sectors*, *Phys. Rev.* **D94** (2016) 063506, [[1604.02401](#)].
- [23] R. A. Flores and J. R. Primack, *Observational and theoretical constraints on singular dark matter halos*, *Astrophys.J.* **427** (1994) L1–4, [[astro-ph/9402004](#)].
- [24] B. Moore, *Evidence against dissipationless dark matter from observations of galaxy haloes*, *Nature* **370** (1994) 629.
- [25] S.-H. Oh, C. Brook, F. Governato, E. Brinks, L. Mayer et al., *The central slope of dark matter cores in dwarf galaxies: Simulations vs. THINGS*, *Astron.J.* **142** (2011) 24, [[1011.2777](#)].
- [26] M. G. Walker and J. Peñarrubia, *A Method for Measuring (Slopes of) the Mass Profiles of Dwarf Spheroidal Galaxies*, *Astrophys. J.* **742** (2011) 20, [[1108.2404](#)].
- [27] M. Boylan-Kolchin, J. S. Bullock and M. Kaplinghat, *Too big to fail? The puzzling darkness of massive Milky Way subhaloes*, *Mon.Not.Roy.Astron.Soc.* **415** (2011) L40, [[1103.0007](#)].
- [28] S. Garrison-Kimmel, M. Boylan-Kolchin, J. S. Bullock and E. N. Kirby, *Too Big to Fail in the Local Group*, *Mon.Not.Roy.Astron.Soc.* **444** (2014) 222, [[1404.5313](#)].
- [29] D. N. Spergel and P. J. Steinhardt, *Observational evidence for self-interacting cold dark matter*, *Phys.Rev.Lett.* **84** (2000) 3760–3763, [[astro-ph/9909386](#)].
- [30] B. D. Wandelt, R. Dave, G. R. Farrar, P. C. McGuire, D. N. Spergel et al., *Self-interacting dark matter*, in *Sources and Detection of Dark Matter and Dark Energy in the Universe*, pp. 263–274, 2000. [astro-ph/0006344](#).
- [31] M. Vogelsberger, J. Zavala and A. Loeb, *Subhaloes in Self-Interacting Galactic Dark Matter Haloes*, *Mon.Not.Roy.Astron.Soc.* **423** (2012) 3740, [[1201.5892](#)].
- [32] M. Rocha, A. H. Peter, J. S. Bullock, M. Kaplinghat, S. Garrison-Kimmel et al., *Cosmological Simulations with Self-Interacting Dark Matter I: Constant Density Cores and Substructure*, *Mon.Not.Roy.Astron.Soc.* **430** (2013) 81–104, [[1208.3025](#)].
- [33] A. H. Peter, M. Rocha, J. S. Bullock and M. Kaplinghat, *Cosmological Simulations with Self-Interacting Dark Matter II: Halo Shapes vs. Observations*, *Mon.Not.Roy.Astron.Soc.* **430** (2012) 105–120, [[1208.3026](#)].
- [34] J. Zavala, M. Vogelsberger and M. G. Walker, *Constraining Self-Interacting Dark Matter with the Milky Way’s dwarf spheroidals*, *Mon.Not.Roy.Astron.Soc.: Letters* **431** (2013) L20–L24, [[1211.6426](#)].
- [35] M. Vogelsberger, J. Zavala, C. Simpson and A. Jenkins, *Dwarf galaxies in CDM and SIDM with baryons: observational probes of the nature of dark matter*, *Mon. Not. Roy. Astron. Soc.* **444** (2014) 3684, [[1405.5216](#)].

- [36] O. D. Elbert, J. S. Bullock, S. Garrison-Kimmel, M. Rocha, J. Oñorbe and A. H. G. Peter, *Core Formation in Dwarf Halos with Self Interacting Dark Matter: No Fine-Tuning Necessary*, *Mon. Not. Roy. Astron. Soc.* **453** (2015) 29, [[1412.1477](#)].
- [37] M. Kaplinghat, S. Tulin and H.-B. Yu, *Dark Matter Halos as Particle Colliders: Unified Solution to Small-Scale Structure Puzzles from Dwarfs to Clusters*, *Phys. Rev. Lett.* **116** (2016) 041302, [[1508.03339](#)].
- [38] M.-M. Mac Low and A. Ferrara, *Starburst - driven mass loss from dwarf galaxies: Efficiency and metal ejection*, *Astrophys. J.* **513** (1999) 142, [[astro-ph/9801237](#)].
- [39] F. Governato et al., *At the heart of the matter: the origin of bulgeless dwarf galaxies and Dark Matter cores*, *Nature* **463** (2010) 203–206, [[0911.2237](#)].
- [40] J. Silk and A. Nusser, *The massive black hole-velocity dispersion relation and the halo baryon fraction: a case for positive AGN feedback*, *Astrophys. J.* **725** (2010) 556–560, [[1004.0857](#)].
- [41] C. A. Vera-Ciro, A. Helmi, E. Starkenburg and M. A. Breddels, *Not too big, not too small: the dark halos of the dwarf spheroidals in the Milky Way*, *Mon. Not. Roy. Astron. Soc.* **428** (2013) 1696, [[1202.6061](#)].
- [42] A. A. Klypin, A. V. Kravtsov, O. Valenzuela and F. Prada, *Where are the missing Galactic satellites?*, *Astrophys. J.* **522** (1999) 82–92, [[astro-ph/9901240](#)].
- [43] B. Moore, S. Ghigna, F. Governato, G. Lake, T. R. Quinn, J. Stadel et al., *Dark matter substructure within galactic halos*, *Astrophys. J.* **524** (1999) L19–L22, [[astro-ph/9907411](#)].
- [44] DES collaboration, K. Bechtol et al., *Eight New Milky Way Companions Discovered in First-Year Dark Energy Survey Data*, *Astrophys. J.* **807** (2015) 50, [[1503.02584](#)].
- [45] DES collaboration, A. Drlica-Wagner et al., *Eight Ultra-faint Galaxy Candidates Discovered in Year Two of the Dark Energy Survey*, *Astrophys. J.* **813** (2015) 109, [[1508.03622](#)].
- [46] S. Koposov et al., *The Luminosity Function of the Milky Way Satellites*, *Astrophys. J.* **686** (2008) 279–291, [[0706.2687](#)].
- [47] P. Jethwa, V. Belokurov and D. Erkal, *The upper bound on the lowest mass halo*, [1612.07834](#).
- [48] D. Clowe, A. Gonzalez and M. Markevitch, *Weak lensing mass reconstruction of the interacting cluster 1E0657-558: Direct evidence for the existence of dark matter*, *Astrophys. J.* **604** (2004) 596–603, [[astro-ph/0312273](#)].
- [49] M. Markevitch, A. Gonzalez, D. Clowe, A. Vikhlinin, L. David et al., *Direct constraints on the dark matter self-interaction cross-section from the merging galaxy cluster 1E0657-56*, *Astrophys. J.* **606** (2004) 819–824, [[astro-ph/0309303](#)].
- [50] S. W. Randall, M. Markevitch, D. Clowe, A. H. Gonzalez and M. Bradač, *Constraints on the Self-Interaction Cross-Section of Dark Matter from Numerical Simulations of the Merging Galaxy Cluster 1E 0657-56*, *Astrophys. J.* **679** (2008) 1173–1180, [[0704.0261](#)].
- [51] D. Harvey, R. Massey, T. Kitching, A. Taylor and E. Tittley, *The non-gravitational interactions of dark matter in colliding galaxy clusters*, *Science* **347** (2015) 1462–1465, [[1503.07675](#)].
- [52] A. Robertson, R. Massey and V. Eke, *Cosmic particle colliders: simulations of self-interacting dark matter with angularly-dependent scattering*, [1612.03906](#).
- [53] D. Tucker-Smith and N. Weiner, *Inelastic dark matter*, *Phys. Rev.* **D64** (2001) 043502, [[hep-ph/0101138](#)].
- [54] M. McCullough and L. Randall, *Exothermic Double-Disk Dark Matter*, *JCAP* **1310** (2013) 058, [[1307.4095](#)].
- [55] K. Agashe, Y. Cui, L. Necib and J. Thaler, *(In)direct Detection of Boosted Dark Matter*, *JCAP* **1410** (2014) 062, [[1405.7370](#)].

- [56] P. S. Bhupal Dev, A. Mazumdar and S. Qutub, *Constraining Non-thermal and Thermal properties of Dark Matter*, *Front.in Phys.* **2** (2014) 26, [[1311.5297](#)].
- [57] G. L. Kane, P. Kumar, B. D. Nelson and B. Zheng, *Dark matter production mechanisms with a nonthermal cosmological history: A classification*, *Phys. Rev.* **D93** (2016) 063527, [[1502.05406](#)].
- [58] L. J. Hall, K. Jedamzik, J. March-Russell and S. M. West, *Freeze-In Production of FIMP Dark Matter*, *JHEP* **03** (2010) 080, [[0911.1120](#)].
- [59] J. McDonald, *Thermally generated gauge singlet scalars as selfinteracting dark matter*, *Phys. Rev. Lett.* **88** (2002) 091304, [[hep-ph/0106249](#)].
- [60] T. R. Slatyer, *The Sommerfeld enhancement for dark matter with an excited state*, *JCAP* **1002** (2010) 028, [[0910.5713](#)].
- [61] K. Schutz and T. R. Slatyer, *Self-Scattering for Dark Matter with an Excited State*, *JCAP* **1501** (2015) 021, [[1409.2867](#)].
- [62] Y. Zhang, *Self-interacting Dark Matter Without Direct Detection Constraints*, *Phys. Dark Univ.* **15** (2017) 82–89, [[1611.03492](#)].
- [63] B. Holdom, *Two  $U(1)$ ’s and Epsilon Charge Shifts*, *Phys. Lett.* **B166** (1986) 196–198.
- [64] R. H. Cyburt, B. D. Fields, K. A. Olive and T.-H. Yeh, *Big Bang Nucleosynthesis: 2015*, *Rev. Mod. Phys.* **88** (2016) 015004, [[1505.01076](#)].
- [65] S. Tremaine and J. E. Gunn, *Dynamical Role of Light Neutral Leptons in Cosmology*, *Phys. Rev. Lett.* **42** (1979) 407–410.
- [66] A. Boyarsky, O. Ruchayskiy and D. Iakubovskyi, *A Lower bound on the mass of Dark Matter particles*, *JCAP* **0903** (2009) 005, [[0808.3902](#)].
- [67] K. Sigurdson, *Hidden Hot Dark Matter as Cold Dark Matter*, [0912.2346](#).
- [68] A. Fradette, M. Pospelov, J. Pradler and A. Ritz, *Cosmological Constraints on Very Dark Photons*, *Phys. Rev.* **D90** (2014) 035022, [[1407.0993](#)].
- [69] H. Davoudiasl, H.-S. Lee and W. J. Marciano, *‘Dark’ Z implications for Parity Violation, Rare Meson Decays, and Higgs Physics*, *Phys. Rev.* **D85** (2012) 115019, [[1203.2947](#)].
- [70] M. Pospelov, A. Ritz and M. B. Voloshin, *Bosonic super-WIMPs as keV-scale dark matter*, *Phys. Rev.* **D78** (2008) 115012, [[0807.3279](#)].
- [71] M.-Y. Wang, A. H. G. Peter, L. E. Strigari, A. R. Zentner, B. Arant, S. Garrison-Kimmel et al., *Cosmological simulations of decaying dark matter: implications for small-scale structure of dark matter haloes*, *Mon. Not. Roy. Astron. Soc.* **445** (2014) 614–629, [[1406.0527](#)].
- [72] Z. Berezhiani, A. D. Dolgov and I. I. Tkachev, *Reconciling Planck results with low redshift astronomical measurements*, *Phys. Rev.* **D92** (2015) 061303, [[1505.03644](#)].
- [73] M. Blennow, S. Clementz and J. Herrero-Garcia, *Self-interacting inelastic dark matter: A viable solution to the small scale structure problems*, [1612.06681](#).
- [74] P. Agrawal, F.-Y. Cyr-Racine, L. Randall and J. Scholtz, *Make Dark Matter Charged Again*, [1610.04611](#).
- [75] S. Profumo, K. Sigurdson and M. Kamionkowski, *What mass are the smallest protohalos?*, *Phys. Rev. Lett.* **97** (2006) 031301, [[astro-ph/0603373](#)].
- [76] T. Bringmann and S. Hofmann, *Thermal decoupling of WIMPs from first principles*, *JCAP* **0704** (2007) 016, [[hep-ph/0612238](#)].
- [77] M. Viel, G. D. Becker, J. S. Bolton and M. G. Haehnelt, *Warm dark matter as a solution to the small scale crisis: New constraints from high redshift Lyman- $\alpha$  forest data*, *Phys. Rev.* **D88** (2013) 043502, [[1306.2314](#)].

- [78] J. Baur, N. Palanque-Delabrouille, C. Yèche, C. Magneville and M. Viel, *Lyman- $\alpha$  Forests cool Warm Dark Matter*, *JCAP* **1608** (2016) 012, [[1512.01981](#)].
- [79] F. Atrio-Barandela and S. Davidson, *Interacting hot dark matter*, *Phys. Rev.* **D55** (1997) 5886–5894, [[astro-ph/9702236](#)].
- [80] F.-Y. Cyr-Racine, R. de Putter, A. Raccanelli and K. Sigurdson, *Constraints on Large-Scale Dark Acoustic Oscillations from Cosmology*, *Phys. Rev.* **D89** (2014) 063517, [[1310.3278](#)].
- [81] M. Pospelov and J. Pradler, *Big Bang Nucleosynthesis as a Probe of New Physics*, *Ann. Rev. Nucl. Part. Sci.* **60** (2010) 539–568, [[1011.1054](#)].
- [82] T. R. Slatyer, *Indirect Dark Matter Signatures in the Cosmic Dark Ages II. Ionization, Heating and Photon Production from Arbitrary Energy Injections*, *Phys. Rev.* **D93** (2016) 023521, [[1506.03812](#)].
- [83] T. R. Slatyer and C.-L. Wu, *General Constraints on Dark Matter Decay from the Cosmic Microwave Background*, *Phys. Rev.* **D95** (2017) 023010, [[1610.06933](#)].
- [84] R. Essig, E. Kuflik, S. D. McDermott, T. Volansky and K. M. Zurek, *Constraining Light Dark Matter with Diffuse X-Ray and Gamma-Ray Observations*, *JHEP* **11** (2013) 193, [[1309.4091](#)].
- [85] XENON10 collaboration, J. Angle et al., *A search for light dark matter in XENON10 data*, *Phys. Rev. Lett.* **107** (2011) 051301, [[1104.3088](#)].
- [86] XENON collaboration, E. Aprile et al., *Low-mass dark matter search using ionization signals in XENON100*, *Phys. Rev.* **D94** (2016) 092001, [[1605.06262](#)].
- [87] R. Essig, A. Manalaysay, J. Mardon, P. Sorensen and T. Volansky, *First Direct Detection Limits on sub-GeV Dark Matter from XENON10*, *Phys. Rev. Lett.* **109** (2012) 021301, [[1206.2644](#)].
- [88] H. An, M. Pospelov, J. Pradler and A. Ritz, *Direct Detection Constraints on Dark Photon Dark Matter*, *Phys. Lett.* **B747** (2015) 331–338, [[1412.8378](#)].
- [89] I. M. Bloch, R. Essig, K. Tobioka, T. Volansky and T.-T. Yu, *Searching for Dark Absorption with Direct Detection Experiments*, [1608.02123](#).
- [90] C. Kouvaris and J. Pradler, *Probing sub-GeV Dark Matter with conventional detectors*, *Phys. Rev. Lett.* **118** (2017) 031803, [[1607.01789](#)].
- [91] XENON100 collaboration, E. Aprile et al., *First Axion Results from the XENON100 Experiment*, *Phys. Rev.* **D90** (2014) 062009, [[1404.1455](#)].
- [92] LUX collaboration, D. S. Akerib et al., *Improved Limits on Scattering of Weakly Interacting Massive Particles from Reanalysis of 2013 LUX Data*, *Phys. Rev. Lett.* **116** (2016) 161301, [[1512.03506](#)].
- [93] XENON collaboration, E. Aprile et al., *Physics reach of the XENON1T dark matter experiment*, *JCAP* **1604** (2016) 027, [[1512.07501](#)].
- [94] P. W. Graham, D. E. Kaplan, S. Rajendran and M. T. Walters, *Semiconductor Probes of Light Dark Matter*, *Phys. Dark Univ.* **1** (2012) 32–49, [[1203.2531](#)].
- [95] R. Essig, M. Fernández-Serra, J. Mardon, A. Soto, T. Volansky and T.-T. Yu, *Direct Detection of sub-GeV Dark Matter with Semiconductor Targets*, *JHEP* **05** (2016) 046, [[1509.01598](#)].
- [96] W. Guo and D. N. McKinsey, *Concept for a dark matter detector using liquid helium-4*, *Phys. Rev.* **D87** (2013) 115001, [[1302.0534](#)].
- [97] K. Schutz and K. M. Zurek, *Detectability of Light Dark Matter with Superfluid Helium*, *Phys. Rev. Lett.* **117** (2016) 121302, [[1604.08206](#)].
- [98] Y. Hochberg, Y. Zhao and K. M. Zurek, *Superconducting Detectors for Superlight Dark Matter*, *Phys. Rev. Lett.* **116** (2016) 011301, [[1504.07237](#)].

- [99] Y. Hochberg, M. Pyle, Y. Zhao and K. M. Zurek, *Detecting Superlight Dark Matter with Fermi-Degenerate Materials*, *JHEP* **08** (2016) 057, [[1512.04533](#)].
- [100] G. G. Raffelt, *Stars as laboratories for fundamental physics*. 1996.
- [101] H. An, M. Pospelov and J. Pradler, *New stellar constraints on dark photons*, *Phys. Lett.* **B725** (2013) 190–195, [[1302.3884](#)].
- [102] J. Redondo and G. Raffelt, *Solar constraints on hidden photons re-visited*, *JCAP* **1308** (2013) 034, [[1305.2920](#)].
- [103] J. H. Chang, R. Essig and S. D. McDermott, *Revisiting Supernova 1987A Constraints on Dark Photons*, *JHEP* **01** (2017) 107, [[1611.03864](#)].
- [104] E. Hardy and R. Lasenby, *Stellar cooling bounds on new light particles: plasma mixing effects*, *JHEP* **02** (2017) 033, [[1611.05852](#)].
- [105] CMB-S4 collaboration, K. N. Abazajian et al., *CMB-S4 Science Book, First Edition*, [1610.02743](#).
- [106] CORE collaboration, E. Di Valentino et al., *Exploring Cosmic Origins with CORE: Cosmological Parameters*, [1612.00021](#).
- [107] A. Belyaev, N. D. Christensen and A. Pukhov, *CalcHEP 3.4 for collider physics within and beyond the Standard Model*, *Comput. Phys. Commun.* **184** (2013) 1729–1769, [[1207.6082](#)].
- [108] T. Hahn, *Generating Feynman diagrams and amplitudes with FeynArts 3*, *Comput. Phys. Commun.* **140** (2001) 418–431, [[hep-ph/0012260](#)].
- [109] R. Essig, J. Mardon and T. Volansky, *Direct Detection of Sub-GeV Dark Matter*, *Phys. Rev.* **D85** (2012) 076007, [[1108.5383](#)].